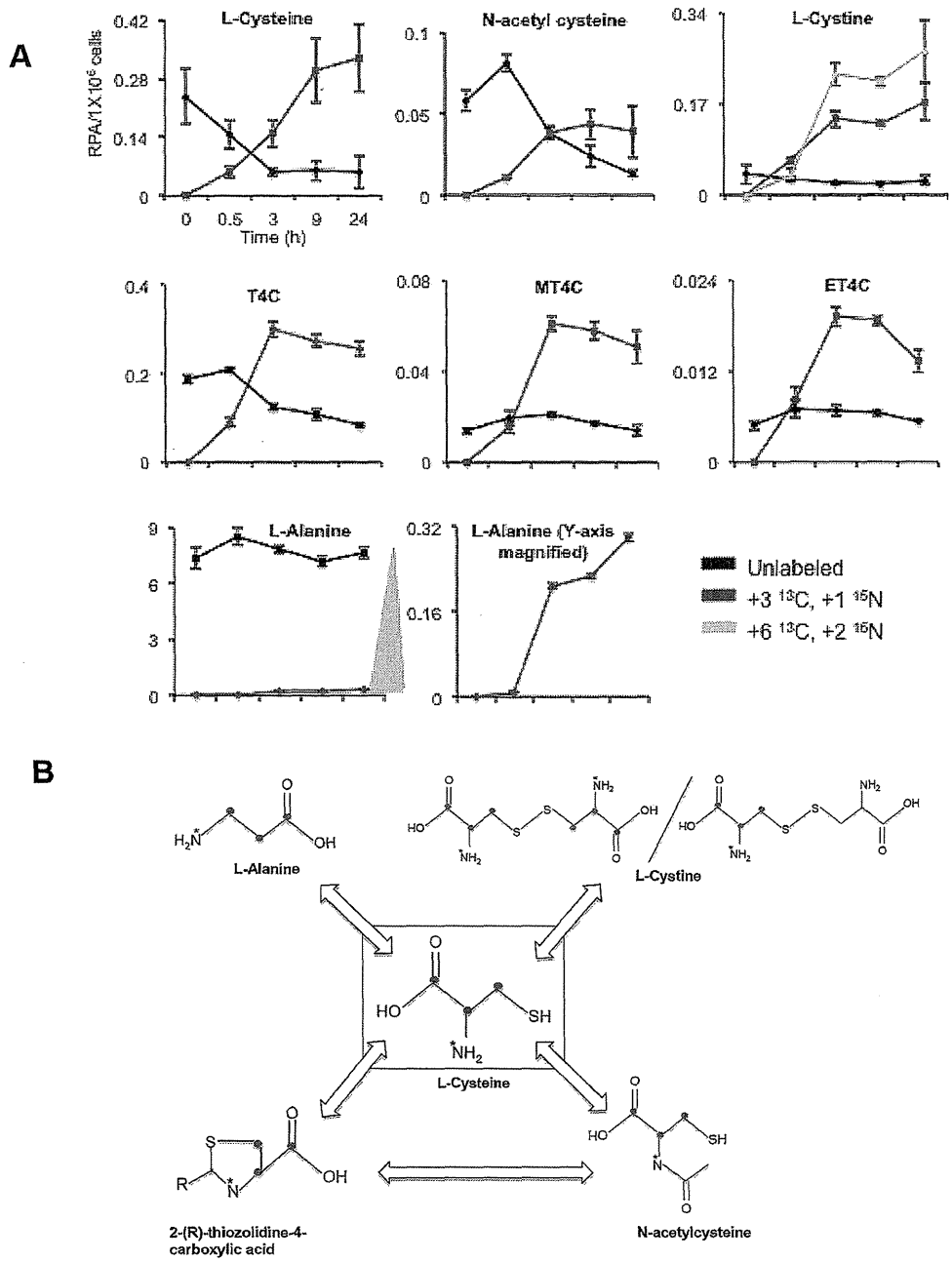

FIG 2 L-Cysteine metabolism in *E. histolytica*. (A) Relative intracellular concentrations of various unlabeled and isotope-labeled L-cysteine-derived metabolites in *E. histolytica* trophozoites. Trophozoites were cultured in the presence of 8 mM stable-isotope-labeled L-cysteine (U-^{13}C3, ^{15}N) in L-cysteine-deprived medium for 0, 0.5, 3, 9, and 24 h. The bottom center plot is a magnified (at the *y* axis) plot of labeled L-alanine, shown at the bottom left. The *x* axis represents time in hours, whereas the *y* axis represents the relative peak areas (RPA) of signal detected with mass spectrometric analysis per 1 × 10^6 cells. Metabolite data are represented as means ± standard deviations (SD) of results from 3 biological replicates. (B) Metabolic flow chart illustrating L-cysteine metabolism in *E. histolytica* trophozoites. Red dots denote ^{13}C atoms, whereas asterisks denote ^{15}N atoms arising from [^{13}C3, ^{15}N1]L-cysteine.

tion of [U-^{13}C3, ^{15}N]L-cysteine to the culture, the levels of [^{13}C3, ^{15}N]L-cysteine increased, and [^{13}C3, ^{15}N]L-cysteine replaced unlabeled L-cysteine after 3 to 9 h (Fig. 2A). L-Cysteine was metabolized into several metabolites. First, L-cysteine was derivatized into three structurally unknown metabolites (see below). Second, L-cysteine was oxidized to L-cystine. The concentration of both [^{13}C3, ^{15}N1]L-cystine and [^{13}C6 ^{15}N2]L-cystine increased up to 24 h, whereas the unlabeled cystine remained constant. The slow and incomplete replacement of unlabeled L-cystine (and also L-cysteine) suggests the presence of an inaccessible pool of L-cysteine and L-cystine in the cell (Fig. 2A). Third, [^{13}C3, ^{15}N1]L-cysteine was metabolized into L-alanine in a reaction catalyzed by

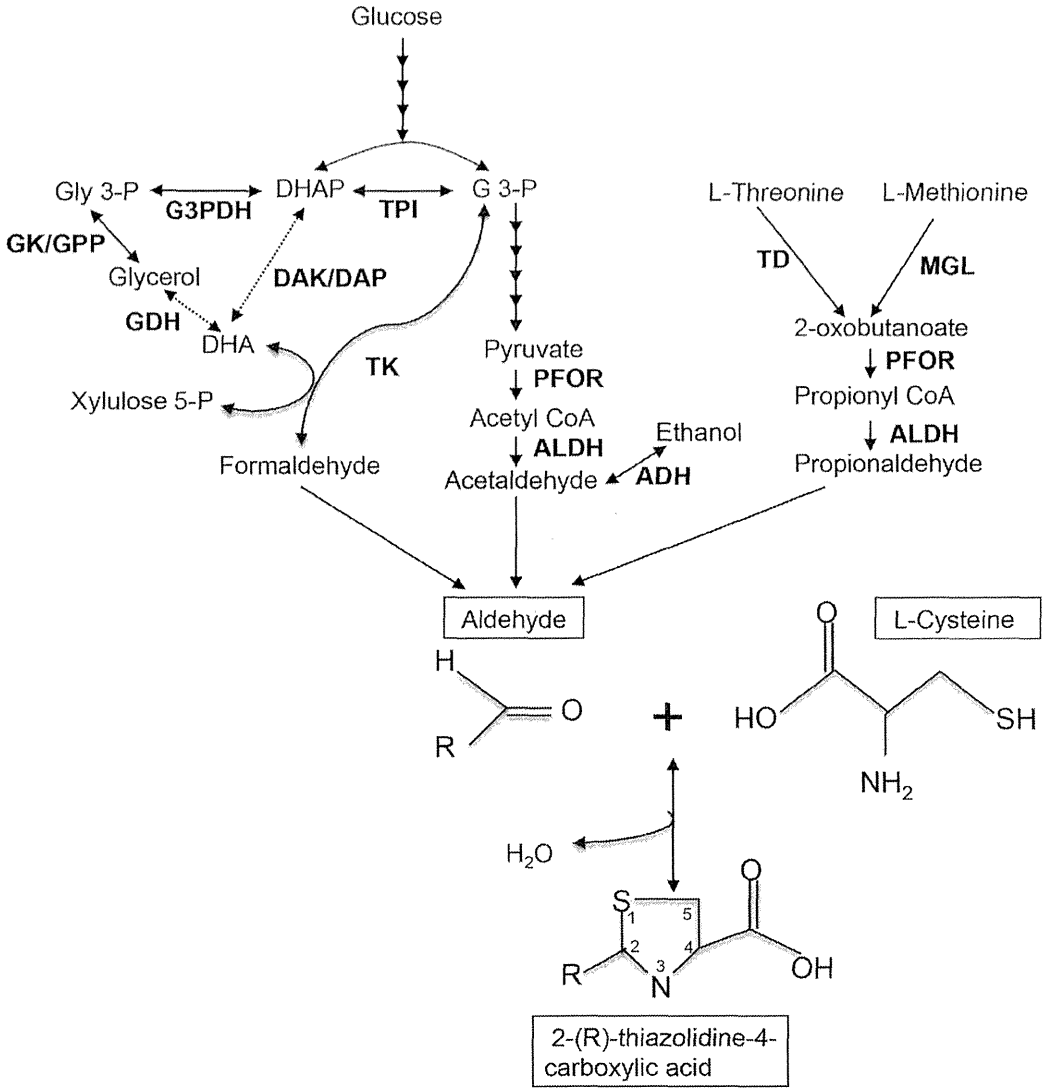

FIG 3 Proposed scheme of 2-(*R*)-thiazolidine-4-carboxylic acid biosynthesis in *E. histolytica* trophozoites. Solid lines represent the steps catalyzed by the enzymes whose genes are present in the genomes, whereas dashed lines indicate those likely absent in the genome or not identified so far. Abbreviations: ADH, alcohol dehydrogenase; ALDH, aldehyde dehydrogenases; CoA, coenzyme A; DAK, dihydroxyacetone kinase; DAP, dihydroxyacetone phosphatase; DHA, dihydroxyacetone; DHAP, dihydroxyacetone phosphate; GDH, glycerol dehydrogenase; GK, glycerol kinase; G 3-P, glyceraldehyde 3-phosphate; G3PDH, glycerol 3-phosphate dehydrogenase; GPP, glycerol 3-phosphate phosphatase; MGL, methionine γ-lyase; PFOR, pyruvate: ferredoxin oxidoreductase; TD, threonine dehydratase; TK, transketolase; TPI, triose phosphate isomerase.

cysteine desulfurase activity, likely by NifS (30). A metabolic flow chart in Fig. 2B depicts incorporation of labels from [U-^{13}C3, ^{15}N1]L-cysteine into the detected metabolites in *E. histolytica* trophozoites.

Discovery of L-cysteine-derived T4Cs in *E. histolytica* trophozoites. We detected three unknown labeled metabolites derived from L-cysteine. These metabolites had never been demonstrated in any protozoan parasites, including *E. histolytica*. Based on the accurate mass measurements, the elemental composition of the metabolites was calculated using the elemental composition calculator (analyst QS software). The elements C, N, O, H, P, and S were automatically considered. After chemical formulas were proposed (see Table S2 in the supplemental material), we searched through a number of databases for the possible compounds and structures, including PubChem (http://pubchem.ncbi.nlm.nih.gov/) and ChemSpider (http://www.chemspider.com/). Finally, their identities were confirmed by comparison to commercially available reference standards (Table S2). The three unknown metabolites were unequivocally identified as thiazolidine-4-carboxylic acid (T4C), 2-methyl thiazolidine-4-carboxylic acid (MT4C), and 2-ethylthiazolidine-4-carboxylic acid (ET4C). The changes in the profiles of these three labeled metabolites were similar; levels of these metabolites increased for up to 3 h and then slightly decreased, suggestive of further conversion or decomposition (Fig. 2A). These metabolites are most likely the condensation products of L-cysteine with aldehydes (Fig. 3). T4C is made of

L-cysteine and formaldehyde (31). In *Entamoeba*, formaldehyde is likely produced by the action of transketolase (Fig. 3). In the *E. histolytica* genome database, we identified five possible transketolase genes (EHI_011410, EHI_002160, EHI_177870, EHI_157770, and EHI_082380). MT4C is the condensation product of L-cysteine with acetaldehyde. Acetaldehyde is a strongly electrophilic compound that is endogenously produced in ethanol metabolism by alcohol dehydrogenase (ADH) (32). Its high reactivity toward biogenic nucleophiles has toxicity as a consequence (33), and thus acetaldehyde needs to be immediately removed from the cell. In *E. histolytica*, acetaldehyde is produced from the fermentation of glucose to ethanol, with pyruvate, acetyl coenzyme A, and acetaldehyde as intermediates (34). *E. histolytica* possesses at least three enzymes with ADH activity. *E. histolytica* ADH1 (EhADH1), which is NADP dependent, shows a marked preference for branched-chain alcohols, whereas EhADH2 prefers ethanol as a substrate (35). It has been reported that EhADH2 may be solely responsible for the conversion of acetyl coenzyme A to acetaldehyde (36). ET4C is formed by condensation of propionaldehyde with L-cysteine. Propionaldehyde in *Entamoeba* is generated through the catabolism of the amino acids L-methionine and L-threonine (Fig. 3).

The formation of these 2-(*R*)-thiazolidine-4-carboxylic acids *in vivo* may therefore provide a possible mechanism for the detoxification of metabolically produced aldehydes in the cell. It was previously reported that at physiological pH, the spontaneous reaction between formaldehyde and L-cysteine to form T4C is rapid and chemically favored (31) and that L-cysteine is immediately directed toward the formation of thiazolidines when these two compounds are added to isolated rat liver homogenate (37), consequently scavenging the toxicity of formaldehyde (38). In rats, T4C was shown to protect the liver against the hepatotoxic effects of ethanol, carbon tetrachloride (39), bromobenzene (40), acetoaminophene (41), tetracycline (42), and thiourea (43). The antiaging effects of T4C were demonstrated in *Drosophila melanogaster* (44) and mice (45), and its antitumor effect was demonstrated clinically (46). It was suggested that T4C is an effective nitrite-trapping agent in the human body and may block endogenous formation of carcinogenic *N*-nitroso compounds (47). Despite evidence from such studies, the metabolic fate of T4C is not well established, except in one study where the metabolic carbon atom of T4C was used as a source for the synthesis of the RNA bases guanine and uracil in *Escherichia coli* (48).

Oxidation and decomposition of T4C. It has previously been shown that T4C is oxidized by *E. coli* (48), rat liver mitochondria (43), and barley (49). Oxidation of T4C by purified rat liver mitochondria yielded *N*-formyl-cysteine as a major end product (43). T4C is first converted to 2,3-thiazoline-4-carboxylate (Fig. 4A), 2,3-thiazolidine-4-carboxylate, and then *N*-acetyl (or formyl or propinyl)-L-cysteine by ring opening and finally gives rise to acetate (or formate or propionate) and L-cysteine by L-proline dehydrogenase (EC 1.5.99.8) (Fig. 4A) (50). Whether an additional enzyme is required to convert *N*-formyl-L-cysteine to formate and L-cysteine is still not clear (50). However, it was suggested that the hydrolysis of *N*-formyl-L-cysteine occurs nonenzymatically (50).

To examine whether these thiazolidine derivatives can liberate L-cysteine in amebic trophozoites, we chose T4C as an example to investigate the fate of these thiazolidine carboxylic acids. We monitored T4C degradation in mixtures of different concentrations (1 to 100 mM) of T4C and amebic lysates. When T4C was incubated with ameba lysates, their time- and dose-dependent increase in the concentration of L-cysteine was observed (Fig. 4B), suggesting that the ameba lysates contain substances such as enzyme(s) that decompose T4C. Since the structure of T4C resembles that of L-proline, with a replacement of a CH_2 group in L-proline by a sulfur atom in T4C (also called thioproline), it was suggested that L-proline dehydrogenase is involved in T4C degradation (50). However, a homologous protein appears to be absent in the *E. histolytica* genome, although more than 55% of the genes in the *E. histolytica* genome remain unannotated (51).

Metabolic fate of T4C, MT4C, and ET4C. In order to further elucidate the metabolic fate of 2-(*R*)-thiazolidine-4-carboxylic acids *in vivo*, we cultured the cell with the medium containing stable-isotope-labeled L-cysteine for 24 h, replaced the medium with the normal BI-S-33 medium lacking L-cysteine, and continued culturing for up to 24 h. A rapid decrease in the concentrations of both labeled and unlabeled MT4C, ET4C, and L-cysteine was observed after a short (0.5-h) lag period (Fig. 4C). We also found a drastic immediate decrease, without a lag period, in the concentrations of labeled T4C and L-cystine (Fig. 4C). Together with the fact that T4C is the most abundant 2-(*R*)-thiazolidine-4-carboxylic acid, this finding suggests that T4C is most immediately accessible and decomposed under L-cysteine deprivation. The fact that the decrease in the L-cystine concentration occurred without a lag period, unlike with L-cysteine, suggests that L-cystine was first reduced to L-cysteine. One of two atypical NADPH-dependent oxidoreductases (EhNO1/2) previously characterized, EhNO2, was shown to catalyze the NADPH-dependent reduction of L-cystine to L-cysteine (11). The changes in the concentrations of labeled and unlabeled *N*-acetyl-L-cysteine were similar to those of L-cysteine, MT4C, and ET4C, reinforcing the premise that MT4C is degraded via *N*-acetyl-L-cysteine and that these thiazolidine derivatives serve as a source of L-cysteine under L-cysteine-deficient conditions, as suggested in rat by Wlodek et al. (52). Neither labeled nor unlabeled *N*-formyl-L-cysteine was detected. This was most likely because their intracellular levels were too low to be detected by CE-TOFMS.

We also found that L-cysteine-derived, labeled L-alanine rapidly decreased under L-cysteine-deprived conditions but that the unlabeled L-alanine concentrations remained approximately 25- to 35-fold higher than those of labeled L-alanine (Fig. 4C). These data indicate that L-cysteine-to-L-alanine conversion by NifS, i.e., iron sulfur cluster formation, is immediately repressed under L-cysteine-deprived conditions. Alternatively, L-alanine produced from L-cysteine is rapidly secreted into the medium, as previously reported (53). It was found that *E. histolytica* also produces L-alanine as a major end product of energy metabolism (53). Although L-alanine may potentially be metabolized into pyruvate by alanine aminotransferase (EC 2.6.1.2), labeled pyruvate was undetectable. These data suggest that this putative alanine aminotransferase may not be functional under the culture conditions tested (data not shown). Since L-alanine is produced through the catabolism of L-cysteine and also as a major end product of energy metabolism in *E. histolytica*, it is conceivable that *Entamoeba* trophozoites excrete L-alanine to expel excess nitrogen out of the cell, as they lack a functional urea cycle (54).

Effect of T4C and MT4C on the growth of *E. histolytica* trophozoites. Previous studies using rats suggested that T4C in a diet may replace L-cystine and L-cysteine to promote growth and pro-

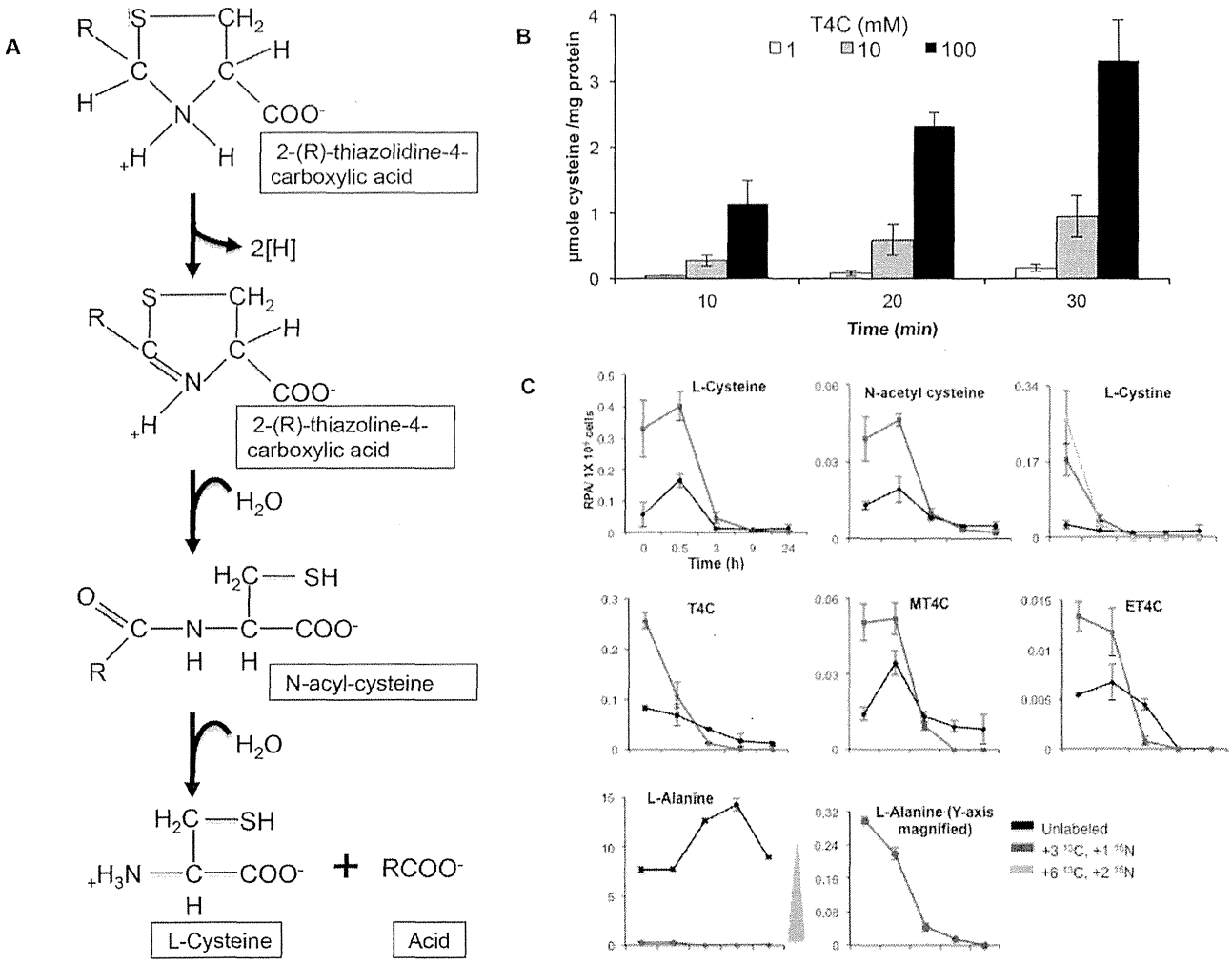

FIG 4 Metabolic decomposition of 2-(*R*)-thiazolidine-4-carboxylic acid in *E. histolytica* trophozoites. (A) Schematic representation of enzymatic degradation of 2-(*R*)-thiazolidine-4-carboxylic acids as previously proposed for *Escherichia coli* by Deutch (50). (B) Time course of T4C's metabolism. The assay was performed as described in Materials and Methods. The means and SD from three independent experiments performed in triplicate are shown. (C) Relative intracellular concentrations of various unlabeled and isotope-labeled metabolites in *E. histolytica* trophozoites. Trophozoites were cultured in the presence of 8 mM stable-isotope-labeled L-cysteine (U-^{13}C3, ^{15}N) for 24 h. Then, stable-isotope-labeled L-cysteine-containing medium was replaced with L-cysteine-deprived BI-S-33 medium, and the trophozoites were harvested at 0, 0.5, 3, 9, and 24 h of cultivation. The bottom center plot is a magnified (at the *y* axis) plot of labeled L-alanine, shown at the bottom left. The *x* axis represents time in hours, whereas the *y* axis represents the relative peak areas per 1×10^6 cells. Metabolite data are presented as means ± SD from 3 biological replicates.

tect the animals against oxidative stress (38, 52). In order to test this premise in *Entamoeba*, we monitored the growth kinetics of trophozoites in the presence and absence of L-cysteine, T4C, or MT4C. As shown in Fig. 5, 2 mM MT4C supported trophozoite growth to an extent almost comparable to that with L-cysteine, and T4C also partially supported growth. In the absence of L-cysteine, T4C, and MT4C, trophozoites showed only negligible growth. The growth-supportive effect of MT4C appears to be higher than that of T4C (Fig. 5), although the intracellular MT4C concentrations were approximately 5-fold lower than those of T4C.

Roles of T4C and MT4C in the antioxidative-stress defense. 2-(*R*)-Thiazolidine-4-carboxylic acids, including T4C are cyclic-sulfur-containing amino acids that are analogous in molecular structure to L-proline. It has been shown that T4C can act as an intracellular sulfhydryl antioxidant and a scavenger of free radicals and thereby protect cellular membranes and other oxidation-prone structures in the cell from damage due to oxygen and oxygen-derived free radicals (55). It was shown that T4C stimulates oxygen uptake in rat liver mitochondria (43). As T4C plays an important role in oxidative-defense mechanisms (55), it was of interest to examine the effect of T4C and MT4C on the amount of intracellular ROS. Our previous study showed that when *E. histolytica* trophozoites were cultured under L-cysteine-limited conditions for 72 h, the intracellular levels of reactive oxygen species increased 4-fold (18). We cultivated trophozoites in L-cysteine-deprived BI-S-33 medium for 72 h, and the medium was replaced with L-cysteine-deprived BI-S-33 medium containing 2 mM T4C, MT4C, or L-cysteine. After 3 h, the relative level of ROS was measured using the fluorescent indicator CM-H $_2$DCFDA [5-(and-6)-

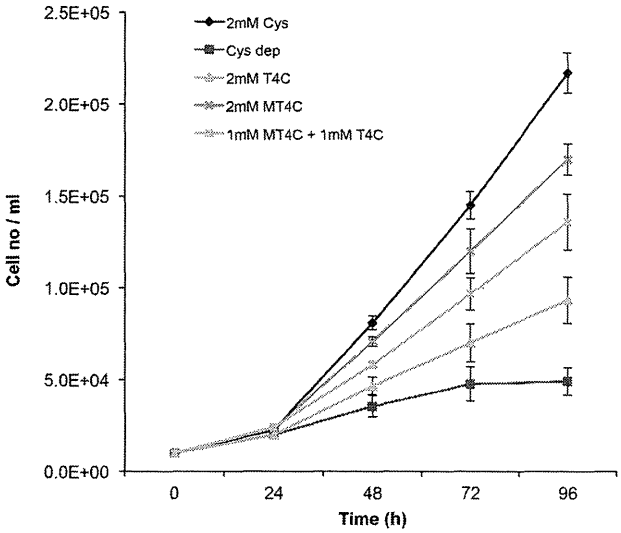

FIG 5 Effect of T4C, MT4C, and L-cysteine on the growth of trophozoites cultured under L-cysteine-depleted conditions. Trophozoites (10^4 cells/ml) were cultivated in L-cysteine-deprived BI-S-33 media with and without 2 mM T4C, MT4C, or L-cysteine or 1 mM each T4C and MT4C. The parasites were counted every 24 h on a hemocytometer. Error bars represent the standard errors of results from five independent experiments. Cys dep, absence of L-cysteine, T4C, and MT4C.

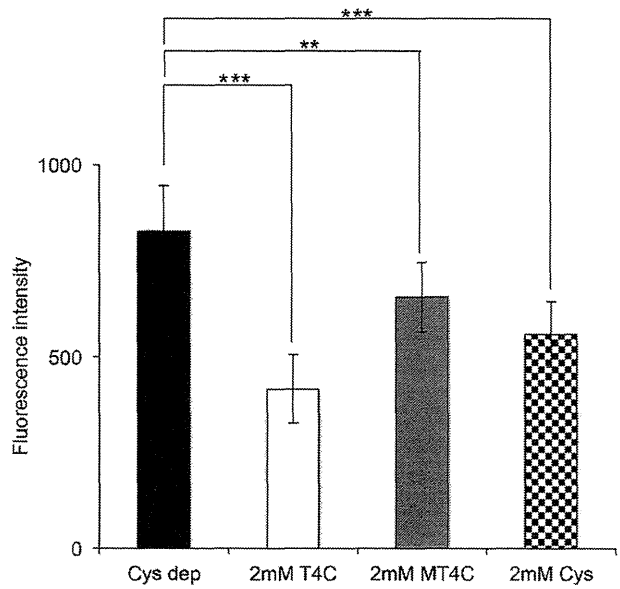

FIG 6 Influence of T4C, MT4C, and L-cysteine on the intracellular ROS levels. Trophozoites were cultivated in L-cysteine-deprived BI-S-33 medium for 72 h, and after that, the medium was replaced with L-cysteine-deprived BI-S-33 media containing 2 mM T4C, MT4C, or L-cysteine. After 3 h, approximately 4.0×10^5 cells were then incubated with the dye 2′,7′-DCF-DA for 20 min. The intracellular ROS levels were quantified by determination of DCF fluorescence. Results were normalized with cell numbers and are presented relative to levels in untreated control cells. The means ± SD from three independent experiments performed in triplicate are shown. Statistical comparisons were made by Student's *t* test (**, $P < 0.01$; ***, $P < 0.001$).

chloromethyl-2′,7′-dichlorodihydrofluorescein diacetate, acetyl ester]. We found that the intracellular levels of reactive oxygen species in trophozoites cultured with 2 mM T4C, MT4C, or L-cysteine were, respectively, approximately 50, 21, or 32% lower than those in control cells (Fig. 6, bar Cys dep). These results suggest that T4C, M4C, and L-cysteine (T4C in particular) are important scavengers of reactive oxygen species in *E. histolytica*. The level of suppression of ROS by supplemented thiazolidine-4-carboxylic acids in the L-cysteine-deprived culture medium was only partial (<50%). This may be because, besides the thiazolidine-4-carboxylic acids described here, L-cysteine-derived metabolites that are involved in the antioxidant defense mechanism may exist in *E. histolytica*. Mackenzie and Harris were the first to recognize the therapeutic potential of T4C in animals (43). They noted that T4C is about five times more potent than L-cysteine in preventing massive pleural effusions and death in thiourea-treated rats. It was presumed that T4C, possessing a protected sulfur atom in its ring, opens and frees a sulfhydryl group after entering a liver cell. L-Cysteine, on the other hand, has an unprotected free sulfhydryl group, which is likely to react with oxidants before entering a cell.

In summary, we found that in *E. histolytica*, L-cysteine is utilized for the synthesis of 2-(*R*)-thiazolidine-4-carboxylic acid derivatives via conjugation with aldehydes. This mechanism allows regulation of the intracellular level of L-cysteine and also functions as a mechanism for detoxifying aldehydes. Our results also suggest that these thiazolidine derivatives serve as storage for L-cysteine, from which L-cysteine can be liberated when required. Furthermore, we have demonstrated that these thiazolidine derivatives, T4C in particular, can reduce the intracellular ROS levels and thus help the parasite to cope with oxidative stress. Future research is needed to determine if these thiazolidine derivatives are also present in other anaerobic/microaerophilic protozoan parasites, such as *Giardia intestinalis* and *Trichomonas vaginalis*, which also require high concentrations of extracellular L-cysteine for growth and survival, in order to verify whether common metabolic and biochemical mechanisms are shared by these parasitic protists in general.

MATERIALS AND METHODS

Chemicals and reagents. All chemicals of analytical grade were purchased from either Wako or Sigma-Aldrich unless otherwise mentioned. 2′,7′-Dichlorodihydrofluorescein diacetate (2′,7′-DCF-DA) was purchased from Invitrogen (U-^{13}C3, ^{15}N). L-Cysteine was purchased from Cambridge Isotope Laboratories. Stock solutions of metabolite standards (1 to 100 mmol/liter) for CE-MS analysis were prepared in either Milli-Q water, 0.1 mol/liter HCl, or 0.1 mol/liter NaOH. A mixed solution of the standards was prepared by diluting stock solutions with Milli-Q water immediately before CE-TOFMS analysis.

Microorganisms and cultivation. Trophozoites of the *E. histolytica* clonal strain HM-1:IMSS cl 6 were maintained axenically in Diamond's BI-S-33 medium at 35.5°C, as described previously (56). Trophozoites were harvested in the late-logarithmic-growth phase 2 to 3 days after the inoculation of medium with 1/30 to 1/12 of the total culture volume.

Metabolic labeling and metabolite extraction. *E. histolytica* trophozoites were cultivated in either standard BI-S-33 medium containing 8 mM L-cysteine or L-cysteine-deprived medium for 48 h. For the metabolic labeling, trophozoites were cultured in the presence of 8 mM stable-isotope-labeled L-cysteine (U-^{13}C3, ^{15}N) in L-cysteine-deprived medium. The reason for using 8 mM stable-isotope-labeled cysteine was because in normal BI-S-33 medium, the concentration of cysteine used to culture *E. histolytica* trophozoites is 8 mM cysteine. To extract metabolites, ap-

proximately 1.5×10^6 cells were harvested after 0, 0.5, 3, 9, and 24 h of cultivation in stable-isotope-labeled L-cysteine (U-^{13}C3, ^{15}N) medium. The cells were immediately suspended in 1.6 ml of −75°C methanol to quench metabolic activity. To ensure that experimental artifacts, such as ion suppression, did not lead to misinterpretation of metabolite levels, internal standards, namely, 2-(*N*-morpholino)ethanesulfonic acid, methionine sulfone, and D-camphor-10-sulfonic acid, were added to each sample (18, 57). The samples were then sonicated for 30 s and mixed with 1.6 ml of chloroform and 0.64 ml of deionized water. After being vortexed, the mixture was centrifuged at 4,600 × *g* at 4°C for 5 min. The aqueous layer (1.6 ml) was filtered using an Amicon Ultrafree-MC ultrafilter (Millipore Co., MA) and centrifuged at 9,100 × *g* at 4°C for approximately 2 h. The filtrate was dried and preserved at −80°C until mass spectrometric analysis (58). Prior to the analysis, the sample was dissolved in 20 μl of de-ionized water containing reference compounds (200 μmol/liter each of 3-aminopyrrolidine and trimesic acid).

Instrumentation and CE-TOFMS conditions. Capillary electrophoresis-time of flight mass spectrometry (CE-TOFMS) was performed using an Agilent CE capillary electrophoresis system equipped with an Agilent 6210 time of flight mass spectrometer, Agilent 1100 isocratic high-performance liquid chromatography (HPLC) pump, Agilent G1603A CE-MS adapter kit, and Agilent G1607A CE-electrospray ionization (ESI)-MS sprayer kit (Agilent Technologies, Waldbronn, Germany). The system was controlled by Agilent G2201AA ChemStation software for CE. Data acquisition was performed by Analyst QS software for Agilent TOF (Applied Biosystems, CA; MDS Sciex, Ontario, Canada).

CE-TOFMS conditions for cationic metabolite analysis. Cationic metabolites were separated in a fused-silica capillary column (50-μm internal diameter, 100-cm total length) filled with 1 mol/liter formic acid as the reference electrolyte (59). Sample solution (~3 nl) was injected at 5,000 Pa for 3 s, and a positive voltage of 30 kV was applied. The capillary and sample trays were maintained at 20°C and below 5°C, respectively. Sheath liquid composed of methanol-water (50%, vol/vol) that contained 0.1 μmol/liter hexakis (2,2-difluorothoxy) phosphazene was delivered at 10 μl/min. ESI-TOFMS was operated in the positive-ion mode. The capillary voltage was set at 4 kV, and a flow rate of nitrogen gas (heater temperature, 300°C) was set at 10 lb/in^2 gauge. For TOFMS, the fragmentor voltage, skimmer voltage, and octopole radio frequency voltage (Oct RFV) were set at 75, 50, and 125 V, respectively. An automatic recalibration function was performed using two reference masses of reference standards, a protonated [^{13}C]methanol dimer (*m/z* 66.063061) and a protonated hexakis (2,2-difluorothoxy) phosphazene (*m/z* 622.028963), which provided the lock mass for exact mass measurements. Exact mass data were acquired at the rate of 1.5 Hz over a 50 to 1,000 *m/z* range.

CE-TOFMS conditions for anionic metabolite analysis. Anionic metabolites were separated in a cationic-polymer-coated COSMO(+) capillary column (50-μm internal diameter, 110-cm length) (Nacalai Tesque) filled with 50 mmol/liter ammonium acetate solution (pH 8.5) as the reference electrolyte (60, 61). Sample solution (~30 nl) was injected at 5,000 Pa for 30 s, and a negative voltage of −30 kV was applied. Ammonium acetate (5 mmol/liter) in methanol-water (50%, vol/vol) that contained 0.1 μmol/liter hexakis (2,2-difluorothoxy) phosphazene was delivered as sheath liquid at 10 μl/min. ESI-TOFMS was operated in the negative-ion mode. The capillary voltage was set at 3.5 kV. For TOFMS, the fragmentor voltage, skimmer voltage, and Oct RFV were set at 100, 50, and 200 V, respectively (61). An automatic recalibration function was performed using two reference masses of reference standards: a deprotonated [^{13}C]acetate dimer (*m/z* 120.038339) and an acetate adduct of hexakis (2,2-difluorothoxy) phosphazene (*m/z* 680.035541). The other conditions were identical to those used for the cationic metabolome analysis.

CE-TOFMS data processing. Raw data were processed using the in-house software Masterhands (62). The overall data processing flow consisted of the following steps: noise filtering, baseline removal, migration time correction, peak detection, and integration of the peak area from a 0.02-*m/z*-wide slice of the electropherograms. This process resembled the strategies employed in widely used data processing software for LC-MS and gas chromatography (GC)-MS data analysis, such as MassHunter (Agilent Technologies) and XCMS (63). Subsequently, accurate *m/z* values for each peak were calculated by Gaussian curve fitting in the *m/z* domain, and migration times were normalized using alignment algorithms based on dynamic programming (64, 65). All target metabolites were identified by matching their *m/z* values and normalized migration times with those of standard compounds in the in-house library.

Growth assay of *E. histolytica* trophozoites. Approximately 6×10^4 exponentially growing trophozoites of *E. histolytica* clonal strain HM-1, IMSS cl 6, were inoculated in 6 ml of L-cysteine-deprived BI-S-33 medium containing 2 mM thiazolidine-4-carboxylic acid, 2 mM methylthiazolidine acid, and 2 mM cysteine, and the parasites were counted every 24 h on a hemocytometer.

Thiazolidine-4-carboxylate oxidation assays. T4C oxidation activity was assayed by measuring the production of L-cysteine by ninhydrin reaction and at an absorbance at 560 nm (66). L-Cysteine contents were determined from an L-cysteine standard curve. The assay mixture contained 50 mM Tris-HCl, pH 7.5, 1 to 100 mM T4C, and appropriate amounts of the fractionated parasite lysate in 50 μl of the reaction mixture. The reaction mixture was incubated for 10 to 30 min at 37°C. The reaction was stopped with 10% trichloroacetic acid. After that, 50 μl of glacial acetic acid and 50 μl of freshly prepared ninhydrin reagent were added to each tube and the tubes were incubated at 95°C for 10 min. Finally, all tubes were cooled down on ice and the reaction mixture was diluted with 200 μl of ethanol and measured immediately at 560 nm with a UV/visible-light spectrophotometer (UV-2550; Shimadzu, Tokyo, Japan). Briefly, different concentrations (1 to 100 mM) of T4C were incubated with amebic lysates at 37°C for 10 to 30 min, and the reactions were stopped with 10% trichloroacetic acid. Aliquots of the acid-soluble material were mixed with the acidic ninhydrin reagent and heated. This sequentially resulted in the conversion of *N*-formylcysteine to L-cysteine and the conjugation of L-cysteine with ninhydrin to form a pink product with an absorbance maximum at 560 nm. T4C reacted with the acidic ninhydrin to form an orange product with a maximum absorbance at 430 nm and a small absorbance at 560 nm. T4C also showed some hydrolysis to L-cysteine. Control mixtures lacking amebic lysates served as controls for T4C oxidation.

Quantitation of reactive oxygen species. Fluorescence spectrophotometry was used to measure the production of intracellular reactive oxygen species using 2′,7′-DCF-DA as a probe as previously described (67). Briefly, *E. histolytica* trophozoites were harvested and washed in phosphate-buffered saline (PBS), and approximately 4.0×10^5 cells were then incubated in 1 ml of PBS containing 20 μM 2′,7′-DCF-DA for 20 min at 35.5°C in the dark. The intensity of fluorescence was immediately read at excitation and emission wavelengths of 492 and 517 nm, respectively.

SUPPLEMENTAL MATERIAL

Supplemental material for this article may be found at http://mbio.asm.org/lookup/suppl/doi:10.1128/mBio.01995-14/-/DCSupplemental.

Table S1, XLSX file, 0.04 MB.

Table S2, XLSX file, 0.04 MB.

ACKNOWLEDGMENTS

This work was supported by grants-in-aid for scientific research from the Ministry of Education, Culture, Sports, Science, and Technology of Japan (MEXT) (23117001, 23117005, 23390099), a grant from the Global COE Program from the MEXT, a grant for research on emerging and reemerging infectious diseases from the Ministry of Health, Labour, and Welfare of Japan, and a grant for research to promote the development of anti-AIDS pharmaceuticals from the Japan Health Sciences Foundation (KHA1101) to T.N.

REFERENCES

1. **Nozaki T, Ali V, Tokoro M.** 2005. Sulfur-containing amino acid metabolism in parasitic protozoa. Adv. Parasitol. **60**:1–99. http://dx.doi.org/10.1016/S0065-308X(05)60001-2.
2. **Kessler D.** 2006. Enzymatic activation of sulfur for incorporation into biomolecules in prokaryotes. FEMS Microbiol. Rev. **30**:825–840. http://dx.doi.org/10.1111/j.1574-6976.2006.00036.x.
3. **Beinert H, Holm RH, Münck E.** 1997. Iron-sulfur clusters: nature's modular, multipurpose structures. Science **277**:653–659. http://dx.doi.org/10.1126/science.277.5326.653.
4. **Park S, Imlay JA.** 2003. High levels of intracellular cysteine promote oxidative DNA damage by driving the Fenton reaction. J. Bacteriol. **185**:942–950. http://dx.doi.org/10.1128/JB.185.6.1942-1950.2003.
5. **Stipanuk MH, Dominy JE, Jr, Lee JI, Coloso RM.** 2006. Mammalian cysteine metabolism: new insights into regulation of cysteine metabolism. J. Nutr. **136**:1652S–1659S.
6. **Stanley SL, Jr..** 2003. Amoebiasis. Lancet **361**:1025–1034. http://dx.doi.org/10.1016/S0140-6736(03)12830-9.
7. **Weinbach EC, Diamond LS.** 1974. *Entamoeba histolytica*. I. Aerobic metabolism. Exp. Parasitol. **35**:232–243. http://dx.doi.org/10.1016/0014-4894(74)90027-7.
8. **Mehlotra RK.** 1996. Antioxidant defense mechanisms in parasitic protozoa. Crit. Rev. Microbiol. **22**:295–314. http://dx.doi.org/10.3109/10408419609105484.
9. **Fahey RC, Newton GL, Arrick B, Overdank-Bogart T, Aley SB.** 1984. *Entamoeba histolytica*: a eukaryote without glutathione metabolism. Science **224**:70–72. http://dx.doi.org/10.1126/science.6322306.
10. **Gillin FD, Diamond LS.** 1981. *Entamoeba histolytica* and *Giardia lamblia*: effects of cysteine and oxygen tension on trophozoite attachment to glass and survival in culture media. Exp. Parasitol. **52**:9–17. http://dx.doi.org/10.1016/0014-4894(81)90055-2.
11. **Jeelani G, Husain A, Sato D, Ali V, Suematsu M, Soga T, Nozaki T.** 2010. Two atypical L-cysteine-regulated NADPH-dependent oxidoreductases involved in redox maintenance, L-cystine and iron reduction, and metronidazole activation in the enteric protozoan *Entamoeba histolytica*. J. Biol. Chem. **285**:26889–26899. http://dx.doi.org/10.1074/jbc.M110.106310.
12. **Husain A, Jeelani G, Sato D, Nozaki T.** 2011. Global analysis of gene expression in response to L-cysteine deprivation in the anaerobic protozoan parasite *Entamoeba histolytica*. BMC Genomics **12**:275. http://dx.doi.org/10.1186/1471-2164-12-275.
13. **Loftus B, Anderson I, Davies R, Alsmark UC, Samuelson J, Amedeo P, Roncaglia P, Berriman M, Hirt RP, Mann BJ, Nozaki T, Suh B, Pop M, Duchene M, Ackers J, Tannich E, Leippe M, Hofer M, Bruchhaus I, Willhoeft U, Bhattacharya A, Chillingworth T, Churcher C, Hance Z, Harris B, Harris D, Jagels K, Moule S, Mungall K, Ormond D, Squares R, Whitehead S, Quail MA, Rabbinowitsch E, Norbertczak H, Price C, Wang Z, Guillén N, Gilchrist C, Stroup SE, Bhattacharya S, Lohia A, Foster PG, Sicheritz-Ponten T, Weber C, Singh U, Mukherjee C, El-Sayed NM, Petri WA, Jr, Clark CG, Embley TM, Barrell B, Fraser CM, Hall N.** 2005. The genome of the protist. Parasite *Entamoeba histolytica*. Nature **433**:865–868. http://dx.doi.org/10.1038/nature03291.
14. **Tokoro M, Asai T, Kobayashi S, Takeuchi T, Nozaki T.** 2003. Identification and characterization of two isoenzymes of methionine γ-lyase from Entamoeba histolytica: a key enzyme of sulfur-amino acid degradation in an anaerobic parasitic protest that lacks forward and reverse transsulfuration pathways. J. Biol. Chem. **278**:42717–42727. http://dx.doi.org/10.1074/jbc.M212414200.
15. **Sato D, Yamagata W, Harada S, Nozaki T.** 2008. Kinetic characterization of methionine gamma-lyases from the enteric protozoan parasite *Entamoeba histolytica* against physiological substrates and trifluoromethionine, a promising lead compound against amoebiasis. FEBS J. **275**:548–560. http://dx.doi.org/10.1111/j.1742-4658.2007.06221.x.
16. **Nozaki T, Asai T, Kobayashi S, Ikegami F, Noji M, Saito K, Takeuchi T.** 1998. Molecular cloning and characterization of the genes encoding two isoforms of cysteine synthase in the enteric protozoan parasite *Entamoeba histolytica*. Mol. Biochem. Parasitol. **97**:33–44. http://dx.doi.org/10.1016/S0166-6851(98)00129-7.
17. **Nozaki T, Asai T, Sanchez LB, Kobayashi S, Nakazawa M, Takeuchi T.** 1999. Characterization of the gene encoding serine acetyltransferase, a regulated enzyme of cysteine biosynthesis from the protist parasites Entamoeba histolytica and Entamoeba dispar. Regulation and possible function of the cysteine biosynthetic pathway in Entamoeba. J. Biol. Chem. **274**:32445–32452.
18. **Husain A, Sato D, Jeelani G, Mi-ichi F, Ali V, Suematsu M, Soga T, Nozaki T.** 2010. Metabolome analysis revealed increase in S-methylcysteine and phosphatidylisopropanolamine synthesis upon L-cysteine deprivation in the anaerobic protozoan parasite *Entamoeba histolytica*. J. Biol. Chem. **285**:39160–39170. http://dx.doi.org/10.1074/jbc.M110.167304.
19. **Gillin FD, Diamond LS.** 1981. *Entamoeba histolytica* and *Giardia lamblia*: growth responses to reducing agents. Exp. Parasitol. **51**:382–391. http://dx.doi.org/10.1016/0014-4894(81)90125-9.
20. **Stipanuk MH.** 2004. Sulfur amino acid metabolism: pathways for production and removal of homocysteine and cysteine. Annu. Rev. Nutr. **24**:539–577. http://dx.doi.org/10.1146/annurev.nutr.24.012003.132418.
21. **Ali V, Nozaki T.** 2007. Current therapeutics, their problems, and sulfur-containing-amino-acid metabolism as a novel target against infections by "amitochondriate" protozoan parasites. Clin. Microbiol. Rev. **20**:164–187. http://dx.doi.org/10.1128/CMR.00019-06.
22. **Enos-Berlage JL, Downs DM.** 1999. Biosynthesis of the pyrimidine moiety of thiamine independent of the PurF enzyme (phosphoribosylpyrophosphate amidotransferase) in *Salmonella typhimurium*: incorporation of stable isotope-labeled glycine and formate. J. Bacteriol. **181**:841–848.
23. **Saunders EC, Ng WW, Chambers JM, Ng M, Naderer T, Krömer JO, Likic VA, McConville MJ.** 2011. Isotopomer profiling of *Leishmania mexicana* promastigotes reveals important roles for succinate fermentation and aspartate uptake in tricarboxylic acid cycle (TCA) anaplerosis, glutamate synthesis, and growth. J. Biol. Chem. **286**:27706–27717. http://dx.doi.org/10.1074/jbc.M110.213553.
24. **Macrae JI, Sheiner L, Nahid A, Tonkin C, Striepen B, McConville MJ.** 2012. Mitochondrial metabolism of glucose and glutamine is required for intracellular growth of *Toxoplasma gondii*. Cell Host Microbe **12**:682–692. http://dx.doi.org/10.1016/j.chom.2012.09.013.
25. **Cobbold SA, Vaughan AM, Lewis IA, Painter HJ, Camargo N, Perlman DH, Fishbaugher M, Healer J, Cowman AF, Kappe SH, Llinás M.** 2013. Kinetic flux profiling elucidates two independent acetyl-CoA biosynthetic pathways in *Plasmodium falciparum*. J. Biol. Chem. **288**:36338–36350. http://dx.doi.org/10.1074/jbc.M113.503557.
26. **Creek DJ, Chokkathukalam A, Jankevics A, Burgess KE, Breitling R, Barrett MP.** 2012. Stable isotope-assisted metabolomics for network wide metabolic pathway elucidation. Anal. Chem. **84**:8442–8447. http://dx.doi.org/10.1021/ac3018795.
27. **Eylert E, Schär J, Mertins S, Stoll R, Bacher A, Goebel W, Eisenreich W.** 2008. Carbon metabolism of *Listeria monocytogenes* growing inside macrophages. Mol. Microbiol. **69**:1008–1017. http://dx.doi.org/10.1111/j.1365-2958.2008.06337.x.
28. **Fan TW, Lane AN, Higashi RM, Farag MA, Gao H, Bousamra M, Miller DM.** 2009. Altered regulation of metabolic pathways in human lung cancer discerned by 13 C stable isotope-resolved metabolomics (SIRM). Mol. Cancer **8**:41. http://dx.doi.org/10.1158/1535-7163.TARG-09-A41.
29. **Eylert E, Herrmann V, Jules M, Gillmaier N, Lautner M, Buchrieser C, Eisenreich W, Heuner K.** 2010. Isotopologue profiling of *Legionella pneumophila*. J. Biol. Chem. **285**:22232–22243. http://dx.doi.org/10.1074/jbc.M110.128678.
30. **Ali V, Shigeta Y, Tokumoto U, Takahashi Y, Nozaki T.** 2004. An intestinal parasitic protist, *Entamoeba histolytica*, possesses a non-redundant nitrogen fixation-like system for iron-sulfur cluster assembly under anaerobic conditions. J. Biol. Chem. **279**:16863–16874. http://dx.doi.org/10.1074/jbc.M313314200.
31. **Ratner S, Clarke HT.** 1937. The action of formaldehyde upon cysteine. J. Am. Chem. Soc. **59**:200–209. http://dx.doi.org/10.1021/ja01280a050.
32. **Bullock C.** 1990. The biochemistry of alcohol metabolism-a brief review. Biochem. Educ. **18**:62–66. http://dx.doi.org/10.1016/0307-4412(90)90174-M.
33. **Von Wartburg JP.** 1987. Acute aldehyde syndrome and chronic aldehydism. Mutat. Res. **186**:249–259. http://dx.doi.org/10.1016/0165-1110(87)90007-8.
34. **Lo HS, Reeves RE.** 1978. Pyruvate-to-ethanol pathway in *Entamoeba histolytica*. Biochem. J. **171**:225–230.
35. **Yang W, Li E, Kairong T, Stanley SL, Jr..** 1994. *Entamoeba histolytica* has an alcohol dehydrogenase homologous to the multifunctional adhE gene product of *Escherichia coli*. Mol. Biochem. Parasitol. **64**:253–260. http://dx.doi.org/10.1016/0166-6851(93)00020-A.
36. **Zhang WW, Shen PS, Descoteaux S, Samuelson J.** 1994. Cloning and

expression of the gene for an $NADP^+$-dependent aldehyde dehydrogenase of *Entamoeba histolytica*. Mol. Biochem. Parasitol. 63:157–161. http://dx.doi.org/10.1016/0166-6851(94)90019-1.
37. Cavallini D, DeMarco C, Mondovi B, Trasarti F. 1956. Studies of the metabolism of thiazolidine carboxylic acid by rat liver homogenate. Biochim. Biophys. Acta 22:558–564.
38. Debey HJ, Mackenzie JB, Mackenzie CG. 1958. The replacement by thiazolidine carboxylic acid of exogenous cystine and cysteine. J. Nutr. 66:607–619.
39. Roquebert J, Dufour P, Ploux D. 1975. Action of sulfur compounds derived from cysteine on the hepatotoxic effects of carbon tetrachloride. Bull. Soc. Pharm. Bordeaux 114:7–11.
40. Siegers CP, Strubelt O, Völpel M. 1978. The antihepatotoxic activity of dithiocarb as compared with six other thio compounds in mice. Arch. Toxicol. 41:79–88. http://dx.doi.org/10.1007/BF00351772.
41. Strubelt O, Siegers CP, Schütt A. 1974. The curative effects of cysteamine, cysteine, and dithiocarb in experimental paracetamol poisoning. Arch. Toxicol. 33:55–64.
42. Peres G, Dumas M. 1972. Liver protecting effects of thiazolidine carboxylic acid with respect to tetracycline. Gazz. Med. Ital. 131:276–282.
43. Mackenzie CG, Harris J. 1957. N-formylcysteine synthesis in mitochondria from formaldehyde and L-cysteine via thiazolidine carboxylic acid. J. Biol. Chem. 227:393–406.
44. Miquel J, Fleming J, Economos AC. 1982. Antioxidants, metabolic rate and aging in *Drosophila*. Arch. Gerontol. Geriatr. 1:159–165. http://dx.doi.org/10.1016/0167-4943(82)90016-4.
45. Miquel J, Economos AC. 1979. Favorable effects of the antioxidants sodium and magnesium thiazolidine carboxylate on the vitality and life span of *Drosophila* and mice. Exp. Gerontal 14:279–285.
46. Brugarolas A, Gosalvez M, Gerety RJ. 1980. Treatment of cancer by an inducer of reverse transformation. Lancet ii:68–70.
47. Kurashima Y, Tsuda M, Sugimura T. 1990. Marked formation of thiazolidine-4-carboxylic acid, an effective nitrite trapping agent in vivo, on boiling of dried shiitake mushroom (*Lentinus edodes*). J. Agric. Food Chem. 38:1945–1949. http://dx.doi.org/10.1021/jf00100a015.
48. Unger L, DeMoss RD. 1966. Metabolism of a proline analogue, L-thiazolidine-4-carboxylic acid, by *Escherichia coli*. J. Bacteriol. 91:1564–1569.
49. Elthon TE, Stewart CR. 1984. Effects of the proline analogue l-thiazolidine-4-carboxylic acid on proline metabolism. Plant Physiol. 74:213–218. http://dx.doi.org/10.1104/74.2.213.
50. Deutch CE. 1992. Oxidation of l-thiazolidine-4-carboxylateby l-proline dehydrogenase in *Escherichia coli*. J. Gen. Microbiol. 138:1593–1598. http://dx.doi.org/10.1099/00221287-138-8-1593.
51. Lorenzi HA, Puiu D, Miller JR, Brinkac LM, Amedeo P, Hall N, Caler EV. 2010. New assembly, reannotation and analysis of the *Entamoeba histolytica* genome reveal new genomic features and protein content information. PLoS Negl. Trop Dis. 4:e716. http://dx.doi.org/10.1371/journal.pntd.0000716.
52. Wlodek L, Rommelspacher H, Susilo R, Radomski J, Höfle G. 1993. Thiazolidine derivatives as source of free L-cysteine in rat tissue. Biochem. Pharmacol. 46:1917–1928. http://dx.doi.org/10.1016/0006-2952(93)90632-7.
53. Zuo X, Coombs GH. 1995. Amino acid consumption by the parasitic, amoeboid protists *Entamoeba histolytica* and *E. invadens*. FEMS Microbiol. Lett. 130:253–258. http://dx.doi.org/10.1111/j.1574-6968.1995.tb07728.x.
54. Clark CG, Alsmark UC, Tazreiter M, Saito-Nakano Y, Ali V, Marion S, Weber C, Mukherjee C, Bruchhaus I, Tannich E, Leippe M, Sicheritz-Ponten T, Foster PG, Samuelson J, Noël CJ, Hirt RP, Embley TM, Gilchrist CA, Mann BJ, Singh U, Ackers JP, Bhattacharya S, Bhattacharya A, Lohia A, Guillén N, Duchêne M, Nozaki T, Hall N. 2007. Structure and content of the *Entamoeba histolytica* genome. Adv. Parasitol. 65:51–190. http://dx.doi.org/10.1016/S0065-308X(07)65002-7.
55. Weber HU, Fleming JF, Miquel J. 1982. Thiazolidine-4-carboxylic acid, a physiologic sulfhydryl antioxidant with potential value in geriatric medicine. Arch. Gerontol. Geriatr. 1:299–310. http://dx.doi.org/10.1016/0167-4943(82)90030-9.
56. Diamond LS, Harlow DR, Cunnick CC. 1978. A new medium for the axenic cultivation of *Entamoeba histolytica* and other Entamoeba. Trans. R. Soc. Trop. Med. Hyg. 72:431–432. http://dx.doi.org/10.1016/0035-9203(78)90144-X.
57. Jeelani G, Sato D, Husain A, Escueta-de Cadiz A, Sugimoto M, Soga T, Suematsu M, Nozaki T. 2012. Metabolic profiling of the protozoan parasite *Entamoeba invadens* revealed activation of unpredicted pathway during encystation. PLoS One 7:e37740. http://dx.doi.org/10.1371/journal.pone.0037740.
58. Ohashi Y, Hirayama A, Ishikawa T, Nakamura S, Shimizu K, Ueno Y, Tomita M, Soga T. 2008. Depiction of metabolome changes in histidine-starved *Escherichia coli* by ce-TOFMS. Mol. Biosyst. 4:135–147. http://dx.doi.org/10.1039/b714176a.
59. Soga T, Heiger DN. 2000. Amino acid analysis by capillary electrophoresis electrospray ionization mass spectrometry. Anal. Chem. 72:1236–1241. http://dx.doi.org/10.1021/ac990976y.
60. Soga T, Ueno Y, Naraoka H, Ohashi Y, Tomita M, Nishioka T. 2002. Simultaneous determination of anionic intermediates for *Bacillus subtilis* metabolic pathways by capillary electrophoresis electrospray ionization mass spectrometry. Anal. Chem. 74:2233–2239. http://dx.doi.org/10.1021/ac020064n.
61. Soga T, Igarashi K, Ito C, Mizobuchi K, Zimmermann HP, Tomita M. 2009. Metabolomic profiling of anionic metabolites by CE-MS. Anal. Chem. 81:6165–6174. http://dx.doi.org/10.1021/ac900675k.
62. Sugimoto M, Wong DT, Hirayama A, Soga T, Tomita M. 2010. Capillary electrophoresis mass spectrometry-based saliva metabolomics identified oral, breast and pancreatic cancer-specific profiles. Metabolomics 6:78–95. http://dx.doi.org/10.1007/s11306-009-0178-y.
63. Smith CA, Want EJ, O'Maille G, Abagyan R, Siuzdak G. 2006. XCMS: processing mass spectrometry data for metabolite profiling using nonlinear peak alignment, matching, and identification. Anal. Chem. 78:779–787. http://dx.doi.org/10.1021/ac051437y.
64. Baran R, Kochi H, Saito N, Suematsu M, Soga T, Nishioka T, Robert M, Tomita M. 2006. MathDAMP: a package for differential analysis of metabolite profiles. BMC Bioinformatics 7:530. http://dx.doi.org/10.1186/1471-2105-7-530.
65. Soga T, Baran R, Suematsu M, Ueno Y, Ikeda S, Sakurakawa T, Kakazu Y, Ishikawa T, Robert M, Nishioka T, Tomita M. 2006. Differential metabolomics reveals ophthalmic acid as an oxidative stress biomarker indicating hepatic glutathione consumption. J. Biol. Chem. 281:16768–16776. http://dx.doi.org/10.1074/jbc.M601876200.
66. Gaitonde MK. 1967. A spectrophotometric method for the direct determination of cysteine in the presence of other naturally occurring amino acids. Biochem. J. 104:627–633.
67. Jeelani G, Husain A, Sato D, Soga T, Suematsu M, Nozaki T. 2013. Biochemical and functional characterization of novel NADH kinase in the enteric protozoan parasite *Entamoeba histolytica*. Biochimie 95:309–319. http://dx.doi.org/10.1016/j.biochi.2012.09.034.

EC
Journals.ASM.org

The *Entamoeba histolytica* Dnmt2 Homolog (Ehmeth) Confers Resistance to Nitrosative Stress

Rivi Hertz,[a] Ayala Tovy,[a] Michael Kirschenbaum,[a] Meirav Geffen,[a] Tomoyoshi Nozaki,[b] Noam Adir,[c] Serge Ankri[a]

Department of Molecular Microbiology, Bruce Rappaport Faculty of Medicine, Technion-Israel Institute of Technology, Haifa, Israel[a]; Department of Parasitology, National Institute of Infectious Diseases, Toyama, Tokyo, Japan[b]; Schulich Faculty of Chemistry, Technion-Israel Institute of Technology, Haifa, Israel[c]

Nitric oxide (NO) has antimicrobial properties against many pathogens due to its reactivity as an S-nitrosylating agent. It inhibits many of the key enzymes that are involved in the metabolism and virulence of the parasite *Entamoeba histolytica* through S-nitrosylation of essential cysteine residues. Very little information is available on the mechanism of resistance to NO by pathogens in general and by this parasite in particular. Here, we report that exposure of the parasites to *S*-nitrosoglutathione (GSNO), an NO donor molecule, strongly reduces their viability and protein synthesis. However, the deleterious effects of NO were significantly reduced in trophozoites overexpressing Ehmeth, the cytosine-5 methyltransferase of the Dnmt2 family. Since these trophozoites also exhibited high levels of $tRNA^{Asp}$ methylation, the high levels suggested that Ehmeth-mediated $tRNA^{Asp}$ methylation is part of the resistance mechanism to NO. We previously reported that enolase, another glycolytic enzyme, binds to Ehmeth and inhibits its activity. We observed that the amount of Ehmeth-enolase complex was significantly reduced in GSNO-treated *E. histolytica*, which explains the aforementioned increase of tRNA methylation. Specifically, we demonstrated via site-directed mutagenesis that cysteine residues 228 and 229 of Ehmeth are susceptible to S-nitrosylation and are crucial for Ehmeth binding to enolase and for Ehmeth-mediated resistance to NO. These results indicate that Ehmeth has a central role in the response of the parasite to NO, and they contribute to the growing evidence that NO is a regulator of epigenetic mechanisms.

Amoebiasis is a parasitic infection of the human intestine and is caused by the single-celled protozoa *Entamoeba histolytica*. The disease has a worldwide distribution with substantial morbidity and mortality, and it is one of the three most common causes of death from parasitic disease (1). The clinical spectrum of amoebiasis ranges from asymptomatic infection to colitis, dysentery, or liver abscess. The parasite has two stages in its life cycle: the infective cyst and the invasive trophozoite. In the host, the parasite is exposed to various environmental challenges and is capable of adapting to the demands of its surrounding environment, such as extreme changes in the glucose concentration and the oxidative and nitrosative attacks of the host immune system (2–5).

E. histolytica belongs to the so-called family of "Dnmt2-only" organisms, in that it does not contain any of the canonical DNA methyltransferases (Dnmt1 and Dnmt3). *E. histolytica* Dnmt2 (Ehmeth) is a weak, but genuine, DNA methyltransferase (6–8), and its ability to catalyze $tRNA^{Asp}$ methylation has been recently demonstrated (9). This dual specificity of Ehmeth for DNA and tRNA has also been proposed for the Dnmt2 homolog in *Drosophila melanogaster* (10). Although control of gene expression by Ehmeth has been reported (6), this function is apparently not its most important function (11). Since Ehmeth expression fluctuates significantly (2- to 3-fold) between laboratory strains where its expression is barely detectable and strains isolated from patients, these fluctuations suggest that Ehmeth is associated with the parasite's adaptation to its host (reference 8 and unpublished observations).

While the overall biological functions of Dnmt2/Ehmeth are not yet completely understood, recent work has enabled us to view their expressions in terms of the parasite's survival, longevity, and adaptability to metabolic and oxidative stresses. We have recently reported that glucose starvation, with the help of the glycolytic enzyme enolase, regulates the parasite's methylation status (9). Enolase interacts with the catalytic site of Ehmeth and inhibits its methyltransferase activity. Dnmt2 expression has been implicated as a necessary component for maintaining the normal life span in *D. melanogaster*, and its overexpression induces longevity in fruit flies (12). It has been proposed that the underlying mechanism of extended longevity is an increased resistance to oxidative damage, which has a well-established association with both degenerative diseases and aging (13). Dnmt2 overexpression induces the expression of small heat shock protein (HSP) in *D. melanogaster* (12) and promotes resistance to H_2O_2 exposure in *E. histolytica* (14).

Nitric oxide (NO) is the major cytotoxic molecule that is released by activated macrophages, natural killer cells, and other phagocytic cells for killing *E. histolytica* trophozoites (15). We have previously reported that NO controls the activity of some of the parasite's virulence factors (16, 17). It has also been recently reported that NO triggers stress responses in *E. histolytica* and that NO directly inhibits glycolysis and stimulates cysteine synthase activity (18). Evidence is emerging that NO is also a regulator of epigenetic events, because it can modify components of the chromatin remodelling machinery (19, 20). While knowledge on NO as an epigenetic regulator is increasing (20, 21), little is known about the effects of NO on Dnmt activity in general and on Dnmt2 in particular. It is also not known whether the protective effects of Dnmt2 against oxidative stress or heat shock (22) apply to nitrosative stress (14).

Received 28 January 2014 Accepted 13 February 2014
Published ahead of print 21 February 2014
Address correspondence to Serge Ankri, sankri@tx.technion.ac.il.
Supplemental material for this article may be found at http://dx.doi.org/10.1128/EC.00031-14.

doi:10.1128/EC.00031-14

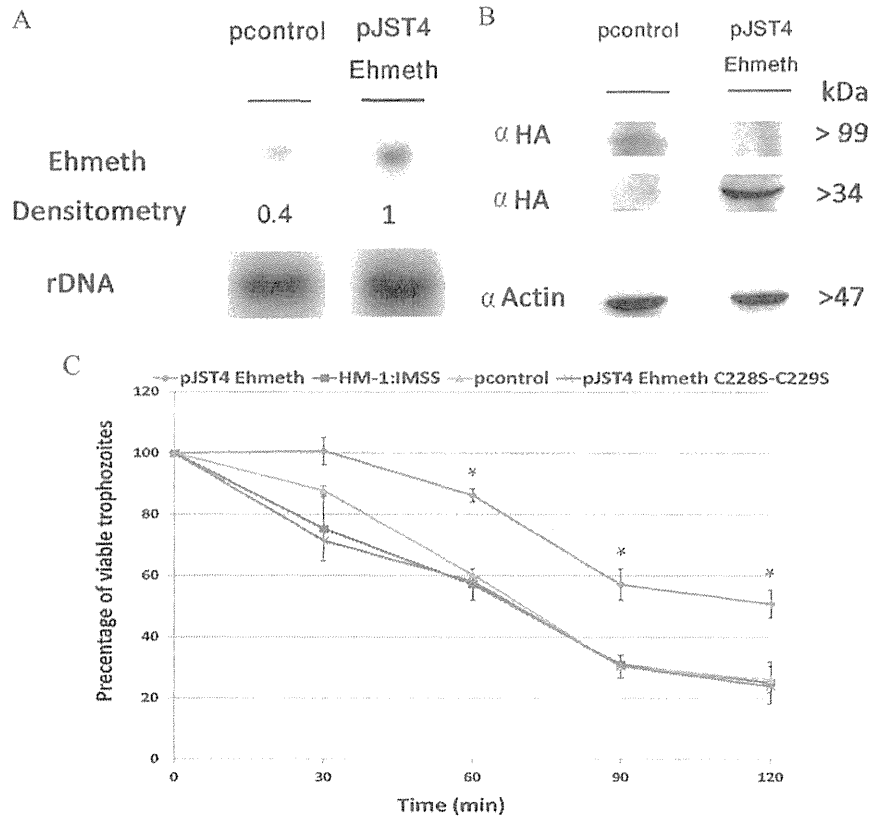

FIG 1 Overexpression of Ehmeth protects *E. histolytica* against nitrosative stress. (A) Northern blot analysis was performed using total RNA that was extracted from pJST4-Ehmeth and pcontrol *E. histolytica* trophozoites. rDNA whose expression was not changed in pJST4-Ehmeth and pcontrol trophozoites were used as controls for RNA loading. The figure displays a representative result from three independent experiments. (B) Western blot analysis was performed on nuclear protein fractions that were prepared from pJST4-Ehmeth and pcontrol *E. histolytica* trophozoites. The proteins were separated on 12% SDS-PAGE gels and analyzed by Western blotting with an anti-HA (α HA) antibody or an anti-actin antibody. The figure displays a representative result from three independent experiments. (C) The viabilities of wild-type *E. histolytica* trophozoites from strain HM-1:MSS, *E. histolytica* trophozoites from a strain that was transfected with a control vector (pcontrol), *E. histolytica* trophozoites that overexpressed Ehmeth (pJST4-Ehmeth), and *E. histolytica* trophozoites that overexpressed pJST4-Ehmeth C228S-C229S exposed to 350 μM GSNO for 30, 60, 90, and 120 min were measured. The number of trophozoites at the beginning of each experiment was set at 100%. Bars represent the standard deviations of the means. The means of the different groups for three independent experiments were compared using Student's *t* test, and statistical significance was set at 5%. The viabilities of the wild-type *E. histolytica* trophozoites of strain HM-1:MSS, the pcontrol *E. histolytica* trophozoites, and the pJST4-Ehmeth C228S-C229S *E. histolytica* trophozoites were not significantly different from each other at any time point, In contrast, the viability of the pJST4-Ehmeth *E. histolytica* trophozoites was significantly different ($P < 0.05$) from that of the wild-type *E. histolytica* trophozoites of strain HM-1:MSS, the pcontrol *E. histolytica* trophozoites, and the pJST4-Ehmeth C228S-C229S *E. histolytica* trophozoites after a 60- or 120-min exposure to GSNO.

In this report, we describe the results of our investigation and describe the underlying molecular mechanisms of increased tolerance to nitrosative stress in *E. histolytica* trophozoites that overexpress Dnmt2. The findings in this report provide the first evidence of NO-mediated regulation of a Dnmt2 protein.

MATERIALS AND METHODS

Microorganisms. *E. histolytica* trophozoites strain HM-1:IMSS were grown under axenic conditions in Diamond's TYI-S-33 medium at 37°C, and trophozoites in the exponential phase of growth were used in all experiments.

Escherichia coli strain BL21(DE3) {F$^-$ *ompT gal dcm lon hsd* S_B(r_B^- m_B^-) λ(DE3 [*lacI lacUV5*-T7 gene 1 *ind1 sam7 min5*])}, a derivative of the *E. coli* B strain, was used for transformation and protein expression.

DNA constructs. The pJST4 expression vector and the pJST4-Klp5 vector (23) were kindly provided by A. Lohia, Department of Biochemistry, Bose Institute, India. The pJST4 expression vector enables the expression of the CHH (calmodulin binding domain, hemagglutin [HA], and histidine [His])-tagged protein in *E. histolytica*; expression of this protein is driven by an actin promoter. The pJST4-Klp5 vector (pcontrol) (23) expresses Klp5, a 99-kDa protein that belongs to the kinesin 5 family (Fig. 1B). This plasmid was used as a control in our previous study in order to exclude the possibility that the CHH tag regulates Ehmeth activity (9), and we used this plasmid for the same purpose in this study. For more details about the construction of pJST4-Ehmeth, see reference 9. The transfection of *E. histolytica* trophozoites was performed using a previously described protocol (14). Details about the construction of the glutathione *S*-transferase (GST)–Ehmeth plasmid were previously described in references 8 and 9.

Site-directed mutagenesis. The expression of the mutagenic plasmids used for recombinant proteins in *E. coli* BL21(DE3), namely, Ehmeth C228S-GST, Ehmeth C229S-GST, and Ehmeth C228S-C229S-GST variants, were created by site-directed mutagenesis. Briefly, pairs of complementary mutagenic primers (Ehmeth C228S 5′ and 3′, Ehmeth C229S 5′ and 3′, and Ehmeth C228S-C229S 5′ and 3′ [Table 1]) were used to amplify the entire GST-Ehmeth plasmid with a high-fidelity non-strand-displacing DNA polymerase (*PFU* DNA polymerase; Promega). The template DNA was eliminated by enzymatic digestion with DpnI, which is

TABLE 1 Primers used in this study

Primer name	Sequence	Direction
Ehmeth C228S 5′	GATAAAAGGACTTCATGTTTTACTAAGTCA	Sense
Ehmeth C228S 3′	TGACTTAGTAAAACATGAAGTCCTTTTATC	Antisense
Ehmeth C229S 5′	AAAAGGACTTGTTCATTTACTAAGTCATAT	Sense
Ehmeth C229S 3′	ATATGACTTAGTAAATGAACAAGTCCTTTT	Antisense
Ehmeth C228S-C229S 5′	GATAAAAGGACTTCATCATTTACTAAGTCA	Sense
Ehmeth C228S-C229S 3′	TGACTTAGTAAATGATGAAGTCCTTTTATC	Antisense
rDNA 5′	ATGGTGAACAATCATACCTT	Sense
rDNA 3′	TTATCGGATGTGTGAGCCC	Antisense
Universal primer	CGCGCGAAGCTTAATACGACTCACTATA	
$tRNA^{Asp}$ primer	TGGCGCTTCAACGGGGATT	

specific for methylated DNA, while the mutated plasmid that was generated *in vitro* was unmethylated and was left undigested. All created mutants were sequenced to ensure the presence of desired mutations and the absence of undesired mutations.

For the expression of CHH-tagged Ehmeth C228S-C229S (pJST4 Ehmeth C228S-C229S) in *E. histolytica*, Ehmeth C228S-C229S was amplified from the plasmid C228S-C229S-GST using the primers Ehmethkpn and EhmethBgl (Table 1) and then cloned in the pJST4 expression vector.

Induction of protein S-nitrosylation. Trophozoites that were grown in Diamond's TYI-S-33 medium were incubated with freshly prepared *S*-nitrosoglutathione (GSNO) solution (350 μM; Sigma-Aldrich) for 1 h at 37°C. The trophozoites were then pelleted by centrifugation at 300 × *g* for 3 min at 4°C, and either total protein extract or total RNA extract was prepared for further analysis.

Northern blotting. For Northern blotting, total RNA was extracted using the RNA isolation kit TRI reagent (Sigma). RNA (10 μg) was separated on a 1% agarose, 0.3% formaldehyde gel in morpholinepropanesulfonic acid (MOPS) buffer (0.2 M MOPS, 50 mM sodium acetate, 5 mM EDTA; pH 7) and then blotted to Genescreen membranes (NEN Bioproducts, Boston, MA). The RNA was cross-linked to the membrane by UV irradiation (1,200 J/cm^2) in a UV Stratalinker apparatus (Stratagene) followed by drying at 80°C for 2 h. The membrane was washed in hybridization buffer (0.5M NaP, 7% SDS, 1 mM EDTA) and then blocked with 100 μg/ml salmon sperm DNA for 1.5 h. Probes were randomly labeled with [α-^{32}P]dCTP by using a random primer DNA labeling mix (Biological Industries, Kibbutz Beit Haemek, Israel) and cleaned on a G-50 column (GE Healthcare). Hybridization with the probes was performed at 60°C overnight. The membrane was then washed several times at 60°C with washing buffer 1 (5% SDS, 40 mM NaP, 1 mM EDTA; pH 7.2), and then with washing buffer 2 (1% SDS, 40 mM NaP, 1 mM EDTA; pH 7.2). The membrane was then exposed to X-ray film (Fujifilm), and the film was developed for detection of the signal.

Western blotting. For Western blotting, nuclear fractions of pJST4-Ehmeth- or pcontrol-transformed *E. histolytica* trophozoites were prepared using a previously described protocol (24). Proteins were resolved on 12% SDS-polyacrylamide gel electrophoresis gels and then transferred to nitrocellulose membranes. Blots were then blocked (3% skim milk powder) and probed with 1:500 mouse monoclonal enolase antibody (sc-271384; Santa Cruz Biotechnology), 1:500 rabbit HA antibody (sc-805; Santa Cruz Biotechnology), or 1:2,000 actin mouse monoclonal antibody (ICN691001; MP Biomedicals) for 16 h at 4°C. After incubation with the first antibody, the blots were incubated with a 1:5,000 dilution of a corresponding second antibody for 1 h at room temperature (Jackson ImmunoResearch) and then developed via enhanced chemiluminescence.

Viability assay under NO stress. *E. histolytica* trophozoites (1 × 10^6) were exposed to 350 μM GSNO for 30, 60, 90, and 120 min. At each time point, an aliquot (10 μl) of the culture was stained with eosin (0.1% final concentration), and the number of living trophozoites was counted in a counting chamber under a light microscope.

tRNA bisulfite sequencing. Total RNA isolation and bisulfite conversions were done using a previously described protocol (25). Bisulfite-treated tRNAs were reverse transcribed by using a tRNA 3′-specific stem-loop primer and amplified with primers that bind only to the deaminated sequences at the 5′ end (Universal primer and Second $tRNA^{Asp}$ primer [Table 1]). Amplicons were subcloned in pGEM-T Easy (Promega) and sequenced (by the Multi-Disciplinary Laboratories Unit, Bruce Rappaport Faculty of Medicine, Technion).

Protein synthesis assay with puromycin. Trophozoites (2 × 10^6/ml) that were treated with either 35 μM or 175 μM GSNO for 15 min at 37°C and untreated control trophozoites were incubated with 10 μg/ml puromycin (Sigma) for 20 min. For pretreatment of the trophozoites with cycloheximide (Sigma), the trophozoites were incubated with 100 μg/ml cycloheximide for 5 min before the addition of puromycin. The trophozoites were lysed with 1% Igepal (Sigma) in phosphate-buffered saline (PBS). Puromycin was detected by immunoblotting with a 12D10 clone monoclonal puromycin antibody (Millipore).

Protein synthesis assay with [^{35}S]methionine. Trophozoites (2 × 10^6/ml) that were grown in Diamond's TYI-S-33 medium were harvested by low-speed centrifugation at room temperature, washed twice with Dulbecco's modified Eagle medium (DMEM) without serum, and then exposed to 350 μM GSNO for 20 min at 37°C. The trophozoites were washed twice again with DMEM without serum and then incubated with 50 μCi/ml [^{35}S]methionine (Sigma) for 2 h at 37°C. The trophozoites were washed twice with PBS and then lysed using 1% Igepal (Sigma) in PBS. Radiolabeled proteins were precipitated on Whatman filter paper by using trichloroacetic acid and were analyzed by liquid scintillation counting.

Proteolysis of protein samples and mass spectrometry analysis. Protein samples were resolved by 12% SDS-polyacrylamide gel electrophoresis. The proteins in each gel slice were reduced with 2.8 mM dithiothreitol (DTT; 60°C for 30 min), modified with 8.8 mM iodoacetamide in 100 mM ammonium bicarbonate in the dark at room temperature for 30 min, and digested overnight in 10% acetonitrile and 10 mM ammonium bicabonate with modified trypsin (Promega) at 37°C. The resulting tryptic peptides were resolved by reverse-phase chromatography on 0.075- by 200-mm fused silica capillaries (J&W) packed with Reprosil reverse-phase material (Dr. Maisch GmbH, Germany). The peptides were eluted with linear gradients of 7 to 40% acetonitrile with 0.1% formic acid in water at a flow rate of 0.25 μl/min over 94 min and 95% acetonitrile with 0.1% formic acid in water at a flow rate of 0.25 μl/min over 12 min. Mass spectrometry (MS) was performed by using an ion trap mass spectrometer (Orbitrap; Thermo) in positive mode and repetitively full MS scan followed by collision-induced dissociation (CID) of the seven most dominant ions selected from the first MS scan.

The mass spectrometry data were analyzed using the MaxQuant 1.4.1.2 software (26), which searched the *E. histolytica* section of the NCBI-nr database with a 1% false-discovery rate, and quantified by label-free analysis using the same software.

Immunoprecipitation assays. Aliquots of nuclear protein fractions (100 μg) were diluted in 20 mM HEPES (pH 7.5), 150 mM NaCl, 0.1% Triton, 10% glycerol (HNTG buffer; 300 μl final volume) and then incubated with protein G-Sepharose beads (10 μl; Sigma) for 30 min at 4°C. Nonspecific interacting proteins were excluded by centrifugation (3,000 rpm at 4°C for 5 min). The supernatant was incubated with either 1:200 HA antibody or enolase antibody for 2 h at 4°C. Following incubation, protein G-Sepharose beads (20 μl) were added to the samples, which were then incubated for 16 h at 4°C. Immunoprecipitated proteins were collected by centrifugation, washed three times with HNTG buffer, and then resolved by 12% SDS-polyacrylamide gel electrophoresis. The proteins were then transferred to nitrocellulose membranes for Western blot analysis and detected with either a mouse monoclonal enolase antibody (sc-271384; Santa Cruz Biotechnology) or a rabbit six-histidine antibody (sc-803; Santa Cruz Biotechnology).

Expression of recombinant Ehmeth and Ehmeth mutant proteins in *E. coli* BL21. *E. coli* BL-21(DE3) cells that were transfected with the respective vectors (GST-Ehmeth, Ehmeth C228S-GST, Ehmeth C229S-

GST, and Ehmeth C228S-C229S-GST) were grown overnight at 37°C in Luria broth (LB) medium that contained 100 μg/ml ampicillin. These precultures were inoculated with a 500 ml of a 1:100 dilution of fresh LB medium that contained 100 μg/ml ampicillin and were further grown for 3 h until the optical density at 600 nm of the medium reached 0.8. These bacteria were induced with 0.5 mM isopropyl-beta-D-thiogalactopyranoside (IPTG) for 16 h at 25°C. At the end of incubation, the induced cells were harvested and lysed in lysis buffer (100 mM KCl, 1 mM DTT, 1 mM phenylmethylsulfonylfluoride, 100 μg/ml lysozyme, and 100 μg/ml leupeptin in PBS). The lysed cells were then sonicated for 5 min with 30-s pulses, with 30 s between each pulsing session. The lysis was completed by adding 1:100 BugBuster protein extraction reagent (Novagen). The lysate was then centrifuged at 2,000 × *g* for 20 min in order to recover the soluble proteins in the supernatant. GST fusion proteins were purified by affinity purification on glutathione-Sepharose beads. The recombinant proteins were then eluted with glutathione elution buffer (50 mM Tris-HCl [pH 8.0], 10 mM glutathione [Sigma]), and their concentrations were measured by using Bradford's method (27).

Exposure of Ehmeth and mutants proteins to GSNO. Aliquots (0.04 nmol) of recombinant protein were treated with 5 μM GSNO for 1 h at 37°C in 20 μl of methylation buffer without DTT (100 mM Tris-HCl [pH 7.5], 5% glycerol, 5 mM $MgCl_2$, and 100 mM NaCl). DTT (20 mM) was added to certain protein samples following their exposure to GSNO to revert their S-nitrosylation. Recombinant proteins were resolved by 12% polyacrylamide gel electrophoresis under native conditions and then transferred to nitrocellulose membranes. Membranes were blocked (3% skim milk powder) and then probed with 1:800 rabbit polyclonal *S*-nitrosocysteine (S-NO-Cys) antibody (N5411; Sigma) for 1 h at room temperature. The membrane were then incubated with 1:5,000 secondary antibody to rabbit IgG (Jackson ImmunoResearch) for 1 h at room temperature and developed by using enhanced chemiluminescence. Ponceau S staining of the blots prior to their blocking was used to control the loading and transfer of the proteins to the membranes.

Molecular docking. The coordinates for the *E. histolytica* enolase structure (GenBank accession number XP_649161.1; PDB ID 3QTP) and the *E. histolytica* methyltransferease EhMeth/Dmnt2 (GenBank accession number XP_655267.2; PDB ID 3QV2) were obtained from the Protein Data Bank (http://www.rcsb.org/pdb/home/home.do). All nonprotein residues were removed prior to the docking procedure. Subunit B of enolase was considered the receptor, because it was larger (438 residues) than Ehmeth (320 residues), which served as the ligand during docking. The protein-protein docking was done using the Hex 6.3 platform (28) and the shape correlation. Similar clusters of docked proteins were obtained using SwarmDock (29) and ClusPro (30). Docked complexes were visualized, and the images were produced using PyMol (http://www.pymol.org/).

RESULTS

Overexpression of Ehmeth protects *E. histolytica* against nitrosative stress. In order to test the hypothesis that Ehmeth is involved in the protection of the parasite against nitrosative stress, we determined the viability of three strains of *E. histolytica* trophozoites, namely, wild-type strain HM-1:MSS, *E. histolytica* trophozoites transfected with pcontrol, and *E. histolytica* trophozoites transfected with pJST4-Ehmeth and that overexpressed Ehmeth, after their exposure to 350 μM GSNO for 120 min. GSNO was selected as the NO donor molecule because it is the main nonprotein *S*-nitrosothiol (SNO) in human cells and extracellular fluids (31).

The overexpression of Ehmeth as a CHH-tagged protein was confirmed by both Northern and Western blotting (Fig. 1A and B). Figure 1C displays the time-dependent changes in viability of the three types of *E. histolytica* trophozoites. After 60 min, the viabilities of the wild-type and pcontrol trophozoites were less than that of the pJST4-Ehmeth trophozoites. These differences in viability were exacerbated after 120 min: only 25% of the wild-type *E. histolytica* trophozoites and pcontrol trophozoites were viable, whereas 50% of the pJST4-Ehmeth trophozoites were viable. These results indicate that Ehmeth contributes toward protecting *E. histolytica* trophozoites against nitrosative stress.

$tRNA^{Asp}$ methylation and protein synthesis in NO-treated trophozoites. Eukaryotic protein synthesis is regulated by a variety of tRNA modifications (32). In addition, stress-specific reprogramming of modified ribonucleosides in tRNA is involved in the selective translation of survival proteins (33). We decided to investigate whether Ehmeth is involved in the mechanism of NO resistance in the parasite. For this purpose, we determined the levels of $tRNA^{Asp}$ methylation and protein synthesis in pcontrol trophozoites and pJST4-Ehmeth trophozoites before and after GSNO treatment.

For determining the level of $tRNA^{Asp}$ methylation, we used a recently developed method that is based on bisulfite sequencing of tRNA and enables direct detection of cytosine methylation in tRNA by accurately localizing the methylated cytosines within the sequence (25). The cytosine 38 residue in $tRNA^{Asp}$ is a well-known substrate of Dnmt2 enzymes (25, 34, 35). Amplicons (PCR products) of $tRNA^{Asp}$ were generated from bisulfite-treated total RNA samples that were extracted from *E. histolytica* strains, and the sequences of several independent amplicons were determined. We observed that cytosine 38 methylation in the pJST4-Ehmeth trophozoites was 5 times greater than that in the pcontrol trophozoites (Fig. 2A). This increase of cysteine 38 methylation in the pJST4-Ehmeth trophozoites that were exposed to 350 μM GSNO for 1 h was even higher (6.7 times) than that in the pcontrol trophozoites (Fig. 2A). There were no differences in the levels of cysteine 38 methylation in the untreated and GSNO-treated pcontrol trophozoites. In contrast, the levels of cysteine 38 methylation in the GSNO-treated pJST4-Ehmeth trophozoites were substantially greater than those in the pJST4-Ehmeth trophozoites that were not exposed to GSNO. We observed 100% methylation of the cytosine 49 residue in the three types of trophozoites, irrespective of whether or not they were exposed to GSNO. These findings suggested that the methylation of the cytosine 49 residue is not catalyzed by Ehmeth (Fig. 2A). We also found complete demethylation of other cytosine residues (32, 33, 37, 48, and 56), and these findings indicated that the bisulfite treatment was efficient (Fig. 2A). Collectively, these results confirm our previous observations about the ability of Ehmeth to methylate $tRNA^{Asp}$ (9) and indicate that Ehmeth is similar to other Dnmt2 proteins in that it methylates the cytosine 38 residue of $tRNA^{Asp}$. Additionally, our results showed an unexpected positive effect of NO on $tRNA^{Asp}$ methylation in the pJST4-Ehmeth trophozoites.

Next, we hypothesized that the hypermethylation of $tRNA^{Asp}$ that we detected in the pJST4-Ehmeth trophozoites promotes protein synthesis. In order to test this hypothesis, we used the surface sensing of translation (SUnSET) technique (36), which uses the antibiotic puromycin (a structural analog of tyrosyl-tRNA) and puromycin antibodies to detect the amount of puromycin that was incorporated into nascent peptide chains.

We observed that pcontrol and pEhmeth trophozoites had comparable rates of protein synthesis under control conditions (Fig. 2B). Treating pcontrol trophozoites with either 35 μM or 175 μM GSNO for 15 min inhibited protein synthesis by 30% and 90%, respectively (Fig. 2B). These inhibitory effects of 35 μM and 175 μM GSNO were less pronounced (10% and 40% inhibition,

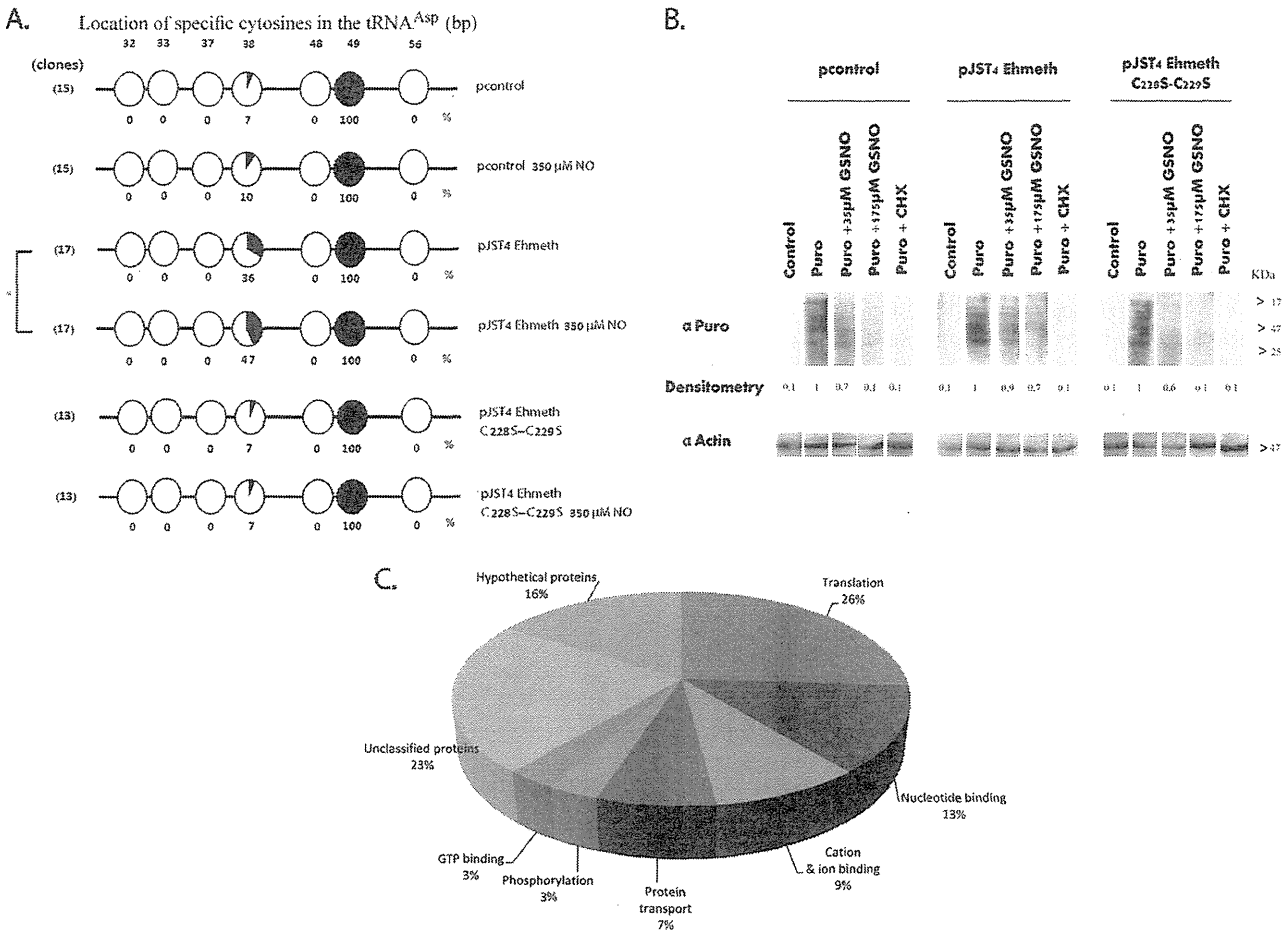

FIG 2 Level of tRNA^{Asp} methylation in NO-treated trophozoites. (A) Bisulfite sequencing analysis of tRNA^{Asp} in pcontrol *E. histolytica* trophozoites, pcontrol *E. histolytica* trophozoites that were treated with 350 μM GSNO for 1 h, pJST4-Ehmeth trophozoites, pJST4 Ehmeth trophozoites treated with GSNO (350 μM for 1 h), pJST4-Ehmeth C228S-C229S trophozoites, and pJST4-Ehmeth C228S-C229S trophozoites treated with GSNO (350 μM for 1 h). The numbers of clones (sequence reads) are displayed in parentheses on the left side of each row. Black areas in the circles indicate methylated cytosine residues, and white areas indicate unmethylated cytosine residues. The percentage of methylated cytosines is indicated below each circle. The location of specific cytosines in the tRNA^{Asp} is indicated under each row. The levels of C38 tRNA^{Asp} methylation in the untreated pcontrol and GSNO-treated pcontrol trophozoites were not significantly different from each other according to the analysis with Student's *t* test, for which statistical significance was set at 5%. In contrast, the levels of C38 tRNA^{Asp} methylation in the untreated and GSNO-treated pJST4 Ehmeth trophozoites were significantly different ($P < 0.05$). (B) Protein synthesis, measured using puromycin-labeled proteins. pcontrol *E. histolytica* trophozoites, pJST4-Ehmeth *E. histolytica* trophozoites, and pJST4-Ehmeth C228S-C229S *E. histolytica* trophozoites were mock treated (control), labeled with 10 μg/ml puromycin (Puro), or treated with 35 μM or 175 μM GSNO for 15 min and then labeled with puromycin for 20 min (Puro + GSNO). Some trophozoites were treated with cycloheximide (CHX; 100 μg/ml) before puromycin labeling (Puro + CHX). The extracts were separated by denaturing electrophoresis and analyzed by Western blotting with a 12D10 clone puromycin antibody. An actin immunoblot is shown as the loading control. The results are representative of two independent experiments. α-Puro, anti-Puro antibody. (C) Functional categories of the upregulated proteins in pJST4-Ehmeth *E. histolytica* trophozoites and pcontrol *E. histolytica* trophozoites exposed to 350 μM GSNO for 1 h. The upregulated proteins were classified according to their biological role based on the David Bioinformatics Resources (http://david.abcc.ncifcrf.gov/).

respectively) in the pJST4-Ehmeth trophozoites (Fig. 2B). Cycloheximide is an inhibitor of protein biosynthesis (37). We also found that the extent of inhibition of protein synthesis by cycloheximide was the same (90%) in the untreated pcontrol and the pJST4-Ehmeth trophozoites. The observation that the inhibitory effect of GSNO in the pJST4-Ehmeth trophozoites was less pronounced than that in the pcontrol trophozoites was confirmed independently by measuring the rate of protein synthesis in these trophozoites by using [^{35}S]methionine (see Fig. S1 in the supplemental material).

We next determined whether Ehmeth overexpression selectively influences the synthesis of proteins that are involved in the resistance to nitrosative stress. For this purpose, we performed quantitative proteomic analysis of pcontrol and pJST4-Ehmeth trophozoites that were exposed or not exposed to 350 μM GSNO for 1 h (see Table S1 in the supplemental material for results of the complete analysis). For the purpose of this study, we decided to focus on proteins that were upregulated in the GSNO-treated pJST4-Ehmeth trophozoites and compare them to those from GSNO-treated pcontrol trophozoites (Fig. 2C). Among these proteins, we identified proteins that are involved in protein translation, such as the 60S and 40S ribosomal proteins and glycyl-tRNA synthetase, protein transport, such as the coatomer beta-subunit and vacuolar sorting protein, and signaling, such as the Rab family

GTPases. Interestingly, two proteins that were significantly upregulated were alcohol dehydrogenase 2 (ADH2; 3-fold increase) and the antioxidant peroxiredoxin (4-fold increase). ADH2 is essential for energy metabolism of oxidatively stressed parasites (38), and peroredoxin has been reported to be associated with resistance to nitrosative stress in *Leishmania* spp. (39).

Collectively, these results strongly suggest that Ehmeth-mediated tRNA methylation has a positive effect on protein synthesis in general and on stress response-related proteins in particular when the parasite is nitrosatively stressed.

The amount of the Ehmeth-enolase inhibitory complex is reduced in NO-treated trophozoites. Although NO usually inhibits enzymatic activity, it can also activate enzymatic activity, as reported for the *E. coli* transcription factors OxyR and SoxR (21). Hence, we decided to investigate whether NO also modulates Ehmeth activity. Ehmeth is devoid of any tRNA methyltransferase activity in the absence of DTT (data not shown). On the other hand, the effect of NO on Ehmeth activity could not be determined in the presence of DTT, because DTT reverses the S-nitrosylation of cysteine.

We previously reported that enolase binds to Ehmeth and inhibits its activity (9). We hypothesized that the hypermethylation of $tRNA^{Asp}$ in NO-treated pJST4-Ehmeth trophozoites (Fig. 2A) is due to reduced formation of the enolase-Ehmeth complex. In order to test this hypothesis, we used trophozoites that were transfected with pJST4-Ehmeth plasmids. In the absence of an efficient Ehmeth antibody, we used an HA antibody to immunoprecipitate Ehmeth and visualized it by Western blotting. Using this approach, which had been previously validated (9), we showed that the amount of Ehmeth-enolase complex in the pJST4-Ehmeth trophozoites that were exposed to 350 μM GSNO for 1 h was significantly lower than that found in the untreated pJST4-Ehmeth trophozoites (Fig. 3A). This result can be explained by either a direct effect of NO on the amount of the Ehmeth-enolase complex or by NO limiting the availability of either one or both of the constituents of the complex. According to the results of Western blot analysis, the amount of Ehmeth did not change in the GSNO-treated parasites (Fig. 3B). Collectively, these results indicate that NO can directly influence the amount of the Ehmeth-enolase complex and the methylation status of $tRNA^{Asp}$.

Although the crystal structure sizes of Ehmeth and enolase have been determined to be 2.15Å and 1.9Å, respectively (40, 41), the molecular details of the Ehmeth-enolase interaction remains uncharacterized.

In order to predict which cysteine residues in Ehmeth are involved in the formation of the Ehmeth-Enolase complex and might be potential targets for S-nitrosylation, we performed an *in silico* docking analysis. Prior to screening for possible complex interfaces, the structures were stripped of nonprotein constituents. The program Hex 6.3 explores the possible energies of protein-protein interactions by using both shape complementarity and electrostatic effects. The top-rated structure, which is displayed in Fig. 4A, showed strong surface complementarity with the loop between residues 250 and 260 of enolase that includes the glutamic acid 253 (Glu253) residue and juts into the aperture that is formed between two globular lobes of the Ehmeth protein. This strong surface complementarity brings the Glu253 residue of enolase into close proximity with the Cys229 residue of Ehmeth. In addition, both the Cys229 residue and its neighbor, the Cys228 residue, of Ehmeth are on a rather unstructured loop, with their

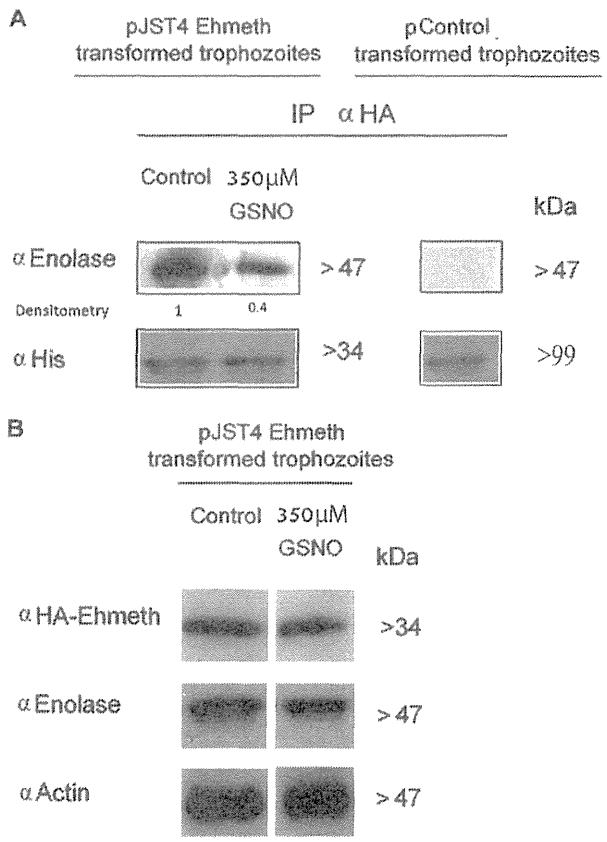

FIG 3 Nitric oxide regulates the amount of Ehmeth-enolase inhibitory complex formed. (A) Ehmeth samples from nuclear lysates of pJST4-Ehmeth and pJST4 Ehmeth *E. histolytica* trophozoites that were treated with 350 μM GSNO for 1 h was immunoprecipitated (IP) with a monoclonal anti-HA (α HA) antibody. The presence of enolase among the immunoprecipitated proteins was detected by Western blotting with an enolase antibody (left). The presence of CHH-tagged Ehmeth among the immunoprecipitated proteins was detected by Western blotting by using a histidine antibody. The immunoprecipitation experiments were also performed with nuclear lysates of pcontrol *E. histolytica* trophozoites as a negative control for the expression of CHH-tagged Ehmeth and for the immunoprecipitation of enolase (right). (B) Western blot analysis of nuclear proteins prepared from GSNO-treated pJST4-Ehmeth and pJST4-Ehmeth *E. histolytica* trophozoites. The proteins were separated on 12% SDS-PAGE gels and analyzed by Western blotting with an HA antibody, an enolase antibody, or an actin antibody. The figure displays a representative result from at least three independent experiments.

SH groups pointing outwards. Hence, the two Cys residues are potentially accessible to NO and to an interacting protein. Figure 4B details the putative interaction between the Glu253 residue of enolase and the Cys229 residue of Ehmeth; the Cys229 residue of Ehmeth was computationally modified by adding NO to the terminal sulfur atom in Fig. 4C.

In Fig. 4D, the complex components have been separated and each protein turned 90° in order to reveal the interaction interface. These interfaces have been overlaid with the surface electrostatic potential, which was calculated using the algorithm in PyMol, a molecular visualization system. This analysis clearly showed that a strong negative potential surrounds the Glu253 residue of enolase, while the area that surrounds the Cys229 residue of Ehmeth is strongly positive.

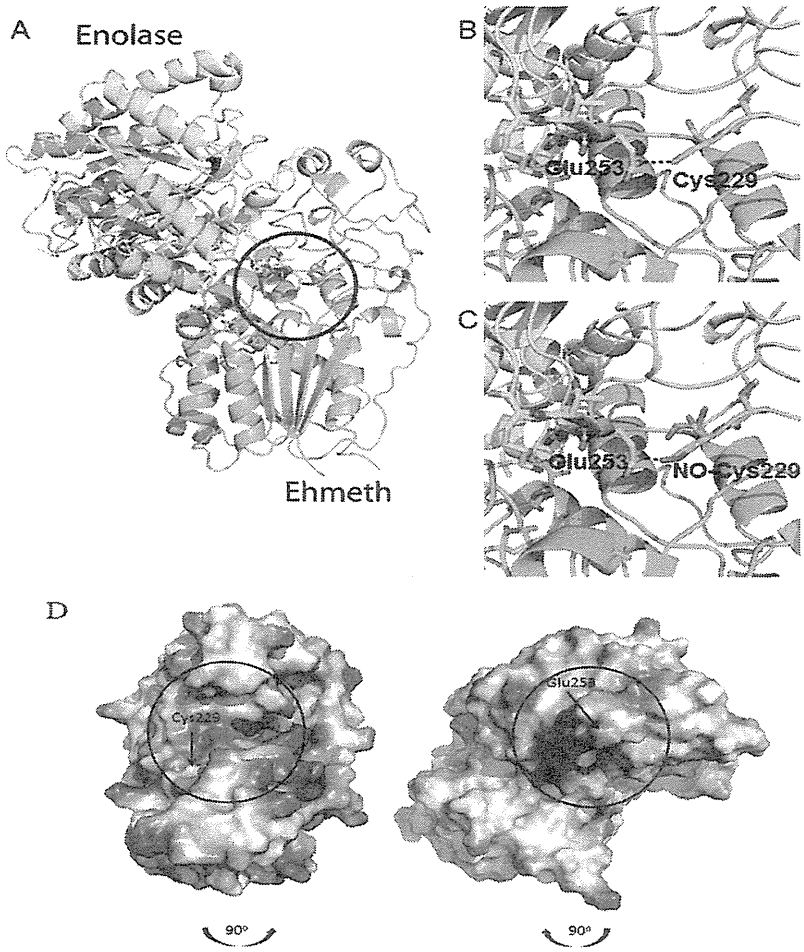

FIG 4 Molecular modeling of the putative enolase-Ehmeth complex. The atomic coordinates of *E. histolytica* enolase and Ehmeth proteins (PDB codes 3QTP and 3QV2, respectively) were docked using the Hex 6.2 platform. (A) The overall best docked structure. (B and C) Close-up images of the interaction between the Glu253 residue of enolase and the Cys229 residue of Ehmeth in the native (B) and NO-modified (C) forms. The complex shown in panel A was disassembled by rotating the enolase 90° in a clockwise direction and the Ehmeth 90° in a counterclockwise direction (the black arrows indicate the direction of complex formation). The interaction interfaces of both proteins are indicated by black circles. (D) Vacuum electrostatic potentials were generated using PyMOL in order to illustrate the charge variance of the *E. histolytica* enolase and Ehmeth proteins, with red and blue indicating negative and positive surfaces, respectively.

Collectively, the output of the *in silico* computer-based modeling of the Ehmeth-enolase interaction suggested that the Cys228 and Cys229 residues are accessible to NO and are important sites for the binding of Ehmeth to enolase.

In order to test the accuracy of this model, we created three Ehmeth mutant proteins: Ehmeth228, Ehmeth229, and Ehmeth228-229, in which the Cys228 residue, the Cys229 residue, and the two cysteine residues were, respectively, replaced with a serine. Following the exposure of the wild-type and mutated proteins to 5 μM GSNO for 1 h, their levels of S-nitrosylation were compared by Western blot analysis by using an S-NO-Cys antibody (Fig. 5A). The presence of S-nitrosylated cysteine(s) was detected in the wild-type Ehmeth protein, but the signal was significantly attenuated in the single mutants and even more so in the double mutants. The specificity of the S-NO-Cys antibody was confirmed by the loss of signal in Ehmeth proteins that were treated with DTT immediately after their S-nitrosylation by GSNO (Fig. 5A). Collectively, these results indicated that Cys228 and Cys229 are efficiently S-nitrosylated.

We next determined the involvement of these cysteines in the formation of the Ehmeth-enolase complex. For this purpose, Ehmeth228-229 was expressed as a CHH-tagged protein in the parasite. According to the results of our Western blot analysis (Fig. 5B), the amounts of Ehmeth and Ehmeth228-229 proteins in the pJST4-Ehmeth and the pJST4-Ehmeth228-229 trophozoites were the same. The amounts of enolase-Ehmeth complex in the pJST4-Ehmeth and the pJST4-Ehmeth228-229 trophozoites were then determined by immunoprecipitation analysis (Fig. 5C). We found that the amount of the Ehmeth-enolase complex in the pJST4-Ehmeth228-229 trophozoites was substantially smaller than that found in the pJST4-Ehmeth trophozoites (Fig. 5C). These results indicated that the Cys228 and Cys229 residues in Ehmeth are involved in the binding of Ehmeth to enolase and strongly suggest that the S-nitrosylation inhibits the formation of the Ehmeth-enolase complex. We next determined the involvement of the Cys228 and Cys229 residues in Ehmeth activity. We found that the levels of $tRNA^{Asp}$ methylation in pcontrol and pJST4-Ehmeth228-229 trophozoites were the same, and this result strongly suggested

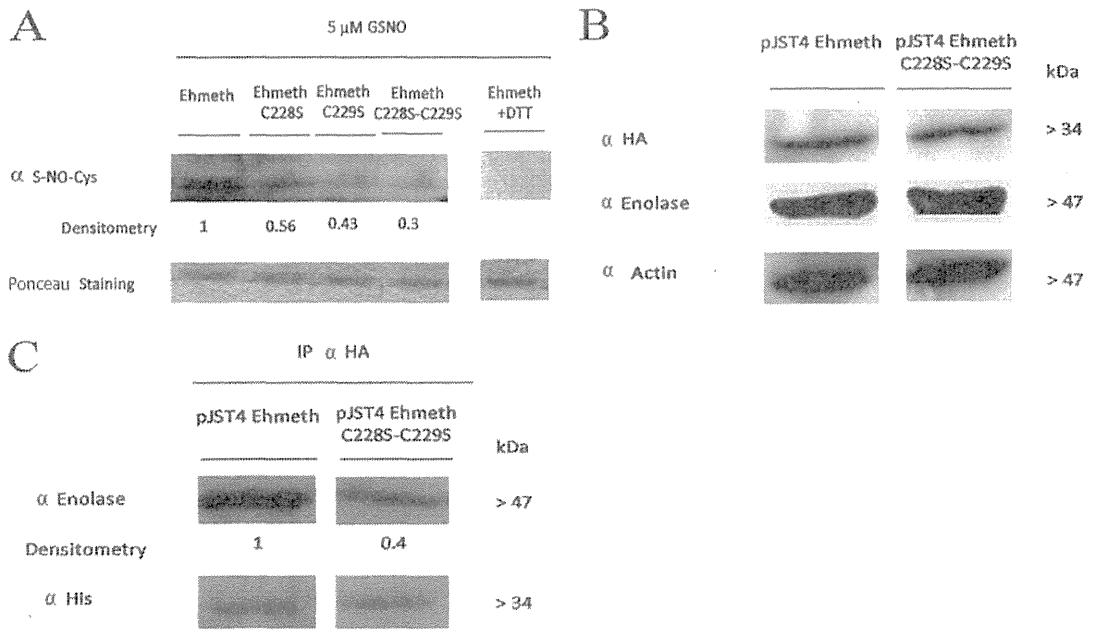

FIG 5 Role of Ehmeth Cys228 and Cys229 in the formation of the Ehmeth-enolase complex. (A) Western blot analysis of recombinant proteins (Ehmeth, Ehmeth C228S, Ehmeth C229S, and Ehmeth C228S-C229S) that were treated with 5 μM GSNO for 1 h at 37°C. The proteins were resolved on 12% polyacrylamide gels under native conditions, transferred to a nitrocellulose membrane, and then probed with an S-NO-Cys antibody (α S-NO-Cys). Ponceau staining of the membrane prior to its interaction with the S-NO-Cys antibody was used as a loading control. The Ehmeth plus DTT control shows the results with the Ehmeth recombinant protein treated with 5 μM GSNO for 1 h at 37°C followed by incubation with 20 mM DTT for 5 min at 37°C. The figure displays a representative result from at least three independent experiments performed singly. (B) Western blot analysis of nuclear protein fractions prepared from pJST4-Ehmeth and pJST4-Ehmeth C228S-C229S *E. histolytica* trophozoites performed using an HA antibody, an enolase antibody, or an actin antibody. The figure displays a representative result from at least three independent experiments performed singly. (C) Immunoprecipitation analysis of Ehmeth from pJST4-Ehmeth and pJST4-Ehmeth C228S-C229S *E. histolytica* trophozoites, performed with an HA antibody. The presence of enolase among the immunoprecipitated proteins was detected by using an enolase antibody. The amounts of Ehmeth and Ehmeth C228S-C229S in the pJST4-Ehmeth and pJST4-Ehmeth C228S-C229S *E. histolytica* trophozoites were determined by using a histidine antibody.

that these mutations impair the catalytic activity of Ehmeth (Fig. 2A). We also found that untreated and GSNO-treated pcontrol and pJST4-Ehmeth228-229 trophozoites had comparable rates of protein synthesis (Fig. 2B), and this result strongly suggested that the level of protein synthesis correlates with the level of $tRNA^{Asp}$ methylation.

Finally, we compared the protective effect of Ehmeth of nitrosatively stressed pJST4 Ehmeth228-229 trophozoites to that of nitrosatively stressed wild-type, pJST4 pcontrol, and pJST4Ehmeth *E. histolytica* trophozoites. We found that the protective effect of Ehmeth in nitrosatively stressed trophozoites was lost when the Ehmeth228-229 protein was overexpressed (Fig. 1C).

DISCUSSION

Mammalian defense strategies against pathogens include the production of a chemical arsenal, such as reactive oxygen and nitrogen species. NO plays a major role in this defense process, and NO-induced inhibition of protein synthesis is part of its cytostatic action in mammalian cells. Different mechanisms, such as NO-mediated cleavage of 28S and 18S rRNA (42) and NO-induced phosphorylation of eukaryotic initiation factor 2α (eIF-2α) (43) have been proposed to explain this inhibitory activity. Therefore, one might surmise that any action of the parasite to counteract the deleterious effect of NO on its protein synthesis is an effective means of resistance against nitrosative stress. Our data indicate the existence of a strong correlation between Ehmeth-mediated tRNA methylation and the control of protein synthesis in nitrosatively stressed *E. histolytica* trophozoites. Most of the recent efforts to explain the role of Dnmt2 in the protection of different organisms from environmental stresses have focused on the organisms' abilities to methylate tRNA (22). Recently, it was proposed that cytosine-5 tRNA methylation in mice promotes tRNA stability and protein synthesis and prevents stress-induced RNase cleavage by angiogenin (44). According to the results of our bioinformatics analysis, the absence of an angiogenin homolog in *E. histolytica* (data not shown) suggests that this protective mechanism does not exist in *E. histolytica*, or that a still-undiscovered RNase in *E. histolytica* has a similar function to that of angiogenin. In contrast, the upregulation of ribosomal proteins 40S and 60S subunits in the GSNO-treated pJST4-Ehmeth trophozoites may be an influential mechanism for maintaining protein synthesis in nitrosatively stressed trophozoites. Our observations are in agreement with the findings of Len and others, indicating that the upregulation of ribosomal proteins 30S and 50S contributes to acid tolerance in *Streptococcus mutans* (45).

The preservation of protein synthesis as a mechanism of resistance against nitrosative stress is somewhat counterintuitive. The general stratagem in most oxidatively stressed and heat-shocked species, including *E. histolytica*, typically includes downregulation of protein synthesis (46, 47) in order to stop energy waste and the toxic buildup of damaged or misfolded proteins. In this investigation, we found paradoxical evidence on the

maintenance of protein synthesis in GSNO-exposed pJST4-Ehmeth trophozoites. We surmise that the additional protein synthesis is a mechanism of titration/competition against the intracellular accumulation of S-nitrosylated proteins. Essentially, an intracellular protein reservoir is created in order to buffer the effects of nitrosative damage. This notion is well illustrated by the fact that the synthesis and turnover of Fe-S cluster-containing proteins in *E. histolytica* that were exposed to the NO donor sodium nitroprusside increased in order to overcome the deleterious effects of NO treatment (18).

Our data indicate that expression of specific stress-related proteins is upregulated in GSNO-treated pJST4-Ehmeth trophozoites. This finding is in agreement with those of Santi-Roca and others (18), who reported that the amount of peroxiredoxin transcripts was increased by NO in *E. histolytica*. It has been reported that ADH2 (48, 49) and peroxiredoxin (50) are associated with the resistance of other organisms to oxidative stress and nitrosative stress (51–53). Accordingly, we posit that these enzymes contribute to the resistance to nitrosative stress of pJST4 Ehmeth trophozoites.

Growing evidence indicates that NO can regulate key epigenetic events, including chromatin remodeling (for a recent review, see reference 21). Our data indicate that S-nitrosylation regulates Dnmt2 activity by inhibiting the formation of an Ehmeth-enolase complex. Since enolase binds to Ehmeth and inhibits its activity (9), this result can be used to explain the significant increase in $tRNA^{Asp}$ methylation that we observed in the GSNO-treated trophozoites. We previously showed that the deletion of the catalytic site in Ehmeth (motif IV) partially suppresses the formation of the Ehmeth-enolase complex, and this finding suggests that other components of Ehmeth are involved in its binding to enolase (9). The results of this investigation shed new light on the formation of this complex and emphasize the importance of the Cys228 and Cys229 residues in Ehmeth in this process. In the future, it will be interesting to challenge and confirm this information for the role of the Glu253 residue of enolase in the formation of the Ehmeth-enolase complex that was obtained in our molecular docking analysis.

In summary, the results of this investigation show that Ehmeth-mediated $tRNA^{Asp}$ methylation is crucial in the protection of *E. histolytica* against nitrosative stress by maintaining active protein synthesis. Another important finding of this study is that NO influences the amount of Ehmeth-enolase complex and consequently regulates Ehmeth activity. The results of this analysis open the door to many important questions about the regulation of Dnmt activity and the role of NO in Dnmt-protein interactions in other organisms. Finally, the results of this investigation indicate that Ehmeth-mediated $tRNA^{Asp}$ methylation is a potential target for development of drugs to treat amoebiasis.

ACKNOWLEDGMENTS

We thank Albert Jeltsch and Tomasz Jurkowski of the Institute of Biochemistry, Stuttgart University, Germany, for their constructive comments, the Smoler Proteomics Center at the Technion for their help with the proteomic analysis of the data, and Arieh Bomzon, ConsulWrite, for his editorial assistance in preparing the manuscript.

This study was supported by grants from the Israel Science Foundation and the Deutsche Forschungsgemeinschaft (DFG).

REFERENCES

1. **Anonymous.** 1997. WHO/PAHO/UNESCO report. A consultation with experts on amoebiasis. Mexico City, Mexico 28–29 January, 1997. Epidemiol. Bull. **18**:13–14.
2. **Baumel-Alterzon S, Weber C, Guillen N, Ankri S.** 2013. Identification of dihydropyrimidine dehydrogenase as a virulence factor essential for the survival of Entamoeba histolytica in glucose-poor environments. Cell. Microbiol. **15**:130–144. http://dx.doi.org/10.1111/cmi.12036.
3. **Tovy A, Hertz R, Siman-Tov R, Syan S, Faust D, Guillen N, Ankri S.** 2011. Glucose starvation boosts Entamoeba histolytica virulence. PLoS Negl. Trop. Dis. **5**(8):e1247. http://dx.doi.org/10.1371/journal.pntd.0001247.
4. **Mortimer L, Chadee K.** 2010. The immunopathogenesis of Entamoeba histolytica. Exp. Parasitol. **126**:366–380. http://dx.doi.org/10.1016/j.exppara.2010.03.005.
5. **Wolfe AJ.** 2005. The acetate switch. Microbiol. Mol. Biol. Rev. **69**:12–50. http://dx.doi.org/10.1128/MMBR.69.1.12-50.2005.
6. **Bernes S, Siman-Tov R, Ankri S.** 2005. Epigenetic and classical activation of Entamoeba histolytica heat shock protein 100 (EHsp100) expression. FEBS Lett. **579**:6395–6402. http://dx.doi.org/10.1016/j.febslet.2005.09.101.
7. **Banerjee S, Fisher O, Lohia A, Ankri S.** 2005. Entamoeba histolytica DNA methyltransferase (Ehmeth) is a nuclear matrix protein that binds EhMRS2, a DNA that includes a scaffold/matrix attachment region (S/MAR). Mol. Biochem. Parasitol. **139**:91–97. http://dx.doi.org/10.1016/j.molbiopara.2004.10.003.
8. **Fisher O, Siman-Tov R, Ankri S.** 2004. Characterization of cytosine methylated regions and 5-cytosine DNA methyltransferase (Ehmeth) in the protozoan parasite Entamoeba histolytica. Nucleic Acids Res. **32**:287–297. http://dx.doi.org/10.1093/nar/gkh161.
9. **Tovy A, Siman Tov R, Gaentzsch R, Helm M, Ankri S.** 2010. A new nuclear function of the Entamoeba histolytica glycolytic enzyme enolase: the metabolic regulation of cytosine-5 methyltransferase 2 (Dnmt2) activity. PLoS Pathog. **6**(2):e1000775. http://dx.doi.org/10.1371/journal.ppat.1000775.
10. **Jurkowski TP, Meusburger M, Phalke S, Helm M, Nellen W, Reuter G, Jeltsch A.** 2008. Human DNMT2 methylates $tRNA^{Asp}$ molecules using a DNA methyltransferase-like catalytic mechanism. RNA **14**:1663–1670. http://dx.doi.org/10.1261/rna.970408.
11. **Ali IK, Ehrenkaufer GM, Hackney JA, Singh U.** 2007. Growth of the protozoan parasite Entamoeba histolytica in 5-azacytidine has limited effects on parasite gene expression. BMC Genomics **8**:7. http://dx.doi.org/10.1186/1471-2164-8-7.
12. **Lin MJ, Tang LY, Reddy MN, Shen CK.** 2005. DNA methyltransferase gene dDnmt2 and longevity of Drosophila. J. Biol. Chem. **280**:861–864. http://dx.doi.org/10.1074/jbc.C400477200.
13. **Zuin A, Castellano-Esteve D, Ayte J, Hidalgo E.** 2010. Living on the edge: stress and activation of stress responses promote lifespan extension. Aging (Albany NY) **2**:231–237.
14. **Fisher O, Siman-Tov R, Ankri S.** 2006. Pleiotropic phenotype in Entamoeba histolytica overexpressing DNA methyltransferase (Ehmeth). Mol. Biochem. Parasitol. **147**:48–54. http://dx.doi.org/10.1016/j.molbiopara.2006.01.007.
15. **Lin JY, Chadee K.** 1992. Macrophage cytotoxicity against Entamoeba histolytica trophozoites is mediated by nitric oxide from L-arginine. J. Immunol. **148**:3999–4005.
16. **Siman-Tov R, Ankri S.** 2003. Nitric oxide inhibits cysteine proteinases and alcohol dehydrogenase 2 of Entamoeba histolytica. Parasitol. Res. **89**:146–149. http://dx.doi.org/10.1007/s00436-002-0716-2.
17. **Elnekave K, Siman-Tov R, Ankri S.** 2003. Consumption of L-arginine mediated by Entamoeba histolytica L-arginase (EhArg) inhibits amoebicidal activity and nitric oxide production by activated macrophages. Parasite Immunol. **25**:597–608. http://dx.doi.org/10.1111/j.0141-9838.2004.00669.x.
18. **Santi-Rocca J, Smith S, Weber C, Pineda E, Hon CC, Saavedra E, Olivos-Garcia A, Rousseau S, Dillies MA, Coppee JY, Guillen N.** 2012. Endoplasmic reticulum stress-sensing mechanism is activated in Entamoeba histolytica upon treatment with nitric oxide. PLoS One **7**:e31777. http://dx.doi.org/10.1371/journal.pone.0031777.
19. **Illi B, Colussi C, Rosati J, Spallotta F, Nanni S, Farsetti A, Capogrossi MC, Gaetano C.** 2011. NO points to epigenetics in vascular development. Cardiovasc. Res. **90**:447–456. http://dx.doi.org/10.1093/cvr/cvr056.
20. **Watson PM, Riccio A.** 2009. Nitric oxide and histone deacetylases: A new

relationship between old molecules. Commun. Integr. Biol. 2:11–13. http://dx.doi.org/10.4161/cib.2.1.7301.
21. Illi B, Colussi C, Grasselli A, Farsetti A, Capogrossi MC, Gaetano C. 2009. NO sparks off chromatin: tales of a multifaceted epigenetic regulator. Pharmacol. Ther. 123:344–352. http://dx.doi.org/10.1016/j.pharmthera.2009.05.003.
22. Schaefer M, Pollex T, Hanna K, Tuorto F, Meusburger M, Helm M, Lyko F. 2010. RNA methylation by Dnmt2 protects transfer RNAs against stress-induced cleavage. Genes Dev. 24:1590–1595. http://dx.doi.org/10.1101/gad.586710.
23. Dastidar PG, Majumder S, Lohia A. 2007. Eh Klp5 is a divergent member of the kinesin 5 family that regulates genome content and microtubular assembly in Entamoeba histolytica. Cell. Microbiol. 9:316–328. http://dx.doi.org/10.1111/j.1462-5822.2006.00788.x.
24. Lavi T, Isakov E, Harony H, Fisher O, Siman-Tov R, Ankri S. 2006. Sensing DNA methylation in the protozoan parasite Entamoeba histolytica. Mol. Microbiol. 62:1373–1386. http://dx.doi.org/10.1111/j.1365-2958.2006.05464.x.
25. Schaefer M, Pollex T, Hanna K, Lyko F. 2009. RNA cytosine methylation analysis by bisulfite sequencing. Nucleic Acids Res. 37:e12. http://dx.doi.org/10.1093/nar/gkn954.
26. Cox J, Mann M. 2008. MaxQuant enables high peptide identification rates, individualized p.p.b.-range mass accuracies and proteome-wide protein quantification. Nat. Biotechnol. 26:1367–1372. http://dx.doi.org/10.1038/nbt.1511.
27. Bradford MM. 1976. A rapid and sensitive method for the quantitation of microgram quantities of protein utilizing the principle of protein-dye binding. Anal. Biochem. 72:248–254.
28. Ritchie DW, Kozakov D, Vajda S. 2008. Accelerating and focusing protein-protein docking correlations using multi-dimensional rotational FFT generating functions. Bioinformatics 24:1865–1873. http://dx.doi.org/10.1093/bioinformatics/btn334.
29. Moal IH, Bates PA. 2010. SwarmDock and the use of normal modes in protein-protein docking. Int. J. Mol. Sci. 11:3623–3648. http://dx.doi.org/10.3390/ijms11103623.
30. Kozakov D, Hall DR, Beglov D, Brenke R, Comeau SR, Shen Y, Li K, Zheng J, Vakili P, Paschalidis I, Vajda S. 2010. Achieving reliability and high accuracy in automated protein docking: ClusPro, PIPER, SDU, and stability analysis in CAPRI rounds 13–19. Proteins. 78:3124–3130. http://dx.doi.org/10.1002/prot.22835.
31. Gaston B, Reilly J, Drazen JM, Fackler J, Ramdev P, Arnelle D, Mullins ME, Sugarbaker DJ, Chee C, Singel DJ, et al. 1993. Endogenous nitrogen oxides and bronchodilator S-nitrosothiols in human airways. Proc. Natl. Acad. Sci. U. S. A. 90:10957–10961.
32. Jackman JE, Alfonzo JD. 2013. Transfer RNA modifications: nature's combinatorial chemistry playground. Wiley Interdiscip Rev. RNA 4:35–48. http://dx.doi.org/10.1002/wrna.1144.
33. Chan CT, Pang YL, Deng W, Babu IR, Dyavaiah M, Begley TJ, Dedon PC. 2012. Reprogramming of tRNA modifications controls the oxidative stress response by codon-biased translation of proteins. Nat. Commun. 3:937. http://dx.doi.org/10.1038/ncomms1938.
34. Goll MG, Kirpekar F, Maggert KA, Yoder JA, Hsieh CL, Zhang X, Golic KG, Jacobsen SE, Bestor TH. 2006. Methylation of $tRNA^{Asp}$ by the DNA methyltransferase homolog Dnmt2. Science 311:395–398. http://dx.doi.org/10.1126/science.1120976.
35. Becker M, Muller S, Nellen W, Jurkowski TP, Jeltsch A, Ehrenhofer-Murray AE. 2012. Pmt1, a Dnmt2 homolog in Schizosaccharomyces pombe, mediates tRNA methylation in response to nutrient signaling. Nucleic Acids Res. 40:11648–11658. http://dx.doi.org/10.1093/nar/gks956.
36. Schmidt EK, Clavarino G, Ceppi M, Pierre P. 2009. SUnSET, a nonradioactive method to monitor protein synthesis. Nat. Methods 6:275–277. http://dx.doi.org/10.1038/nmeth.1314.
37. Korner A. 1966. Effect of cycloheximide on protein biosynthesis in rat liver. Biochem. J. 101:627–631.
38. Pineda E, Encalada R, Rodriguez-Zavala JS, Olivos-Garcia A, Moreno-Sanchez R, Saavedra E. 2010. Pyruvate:ferredoxin oxidoreductase and bifunctional aldehyde-alcohol dehydrogenase are essential for energy metabolism under oxidative stress in Entamoeba histolytica. FEBS J. 277:3382–3395. http://dx.doi.org/10.1111/j.1742-4658.2010.07743.x.
39. Barr SD, Gedamu L. 2003. Role of peroxidoxins in Leishmania chagasi survival. Evidence of an enzymatic defense against nitrosative stress. J. Biol. Chem. 278:10816–10823. http://dx.doi.org/10.1074/jbc.M212990200.
40. Schulz EC, Roth HM, Ankri S, Ficner R. 2012. Structure analysis of Entamoeba histolytica DNMT2 (EhMeth). PLoS One 7:e38728. http://dx.doi.org/10.1371/journal.pone.0038728.
41. Schulz EC, Tietzel M, Tovy A, Ankri S, Ficner R. 2011. Structure analysis of Entamoeba histolytica enolase. Acta Crystallogr. D Biol. Crystallogr. 67:619–627. http://dx.doi.org/10.1107/S0907444911016544.
42. Cai CQ, Guo H, Schroeder RA, Punzalan C, Kuo PC. 2000. Nitric oxide-dependent ribosomal RNA cleavage is associated with inhibition of ribosomal peptidyl transferase activity in ANA-1 murine macrophages. J. Immunol. 165:3978–3984.
43. Kim YM, Son K, Hong SJ, Green A, Chen JJ, Tzeng E, Hierholzer C, Billiar TR. 1998. Inhibition of protein synthesis by nitric oxide correlates with cytostatic activity: nitric oxide induces phosphorylation of initiation factor eIF-2 alpha. Mol. Med. 4:179–190.
44. Tuorto F, Liebers R, Musch T, Schaefer M, Hofmann S, Kellner S, Frye M, Helm M, Stoecklin G, Lyko F. 2012. RNA cytosine methylation by Dnmt2 and NSun2 promotes tRNA stability and protein synthesis. Nat. Struct. Mol. Biol. 19:900–905. http://dx.doi.org/10.1038/nsmb.2357.
45. Len AC, Harty DW, Jacques NA. 2004. Stress-responsive proteins are upregulated in Streptococcus mutans during acid tolerance. Microbiology 150:1339–1351. http://dx.doi.org/10.1099/mic.0.27008-0.
46. Vogel C, Silva GM, Marcotte EM. 2011. Protein expression regulation under oxidative stress. Mol. Cell. Proteomics 10:M111.009217. http://dx.doi.org/10.1074/mcp.M111.009217.
47. Weber C, Guigon G, Bouchier C, Frangeul L, Moreira S, Sismeiro O, Gouyette C, Mirelman D, Coppee JY, Guillen N. 2006. Stress by heat shock induces massive down regulation of genes and allows differential allelic expression of the Gal/GalNAc lectin in Entamoeba histolytica. Eukaryot. Cell 5:871–875. http://dx.doi.org/10.1128/EC.5.5.871-875.2006.
48. Espinosa A, Clark D, Stanley SL, Jr. 2004. Entamoeba histolytica alcohol dehydrogenase 2 (EhADH2) as a target for anti-amoebic agents. J. Antimicrob. Chemother. 54:56–59. http://dx.doi.org/10.1093/jac/dkh280.
49. Espinosa A, Yan L, Zhang Z, Foster L, Clark D, Li E, Stanley SL, Jr. 2001. The bifunctional Entamoeba histolytica alcohol dehydrogenase 2 (EhADH2) protein is necessary for amebic growth and survival and requires an intact C-terminal domain for both alcohol dehydrogenase and acetaldehyde dehydrogenase activity. J. Biol. Chem. 276:20136–20143. http://dx.doi.org/10.1074/jbc.M101349200.
50. Akbar MA, Chatterjee NS, Sen P, Debnath A, Pal A, Bera T, Das P. 2004. Genes induced by a high-oxygen environment in Entamoeba histolytica. Mol. Biochem. Parasitol. 133:187–196. http://dx.doi.org/10.1016/j.molbiopara.2003.10.006.
51. Bryk R, Griffin P, Nathan C. 2000. Peroxynitrite reductase activity of bacterial peroxiredoxins. Nature 407:211–215. http://dx.doi.org/10.1038/35025109.
52. Echave P, Tamarit J, Cabiscol E, Ros J. 2003. Novel antioxidant role of alcohol dehydrogenase E from Escherichia coli. J. Biol. Chem. 278:30193–30198. http://dx.doi.org/10.1074/jbc.M304351200.
53. Vuorinen K, Ohlmeier S, Lepparanta O, Salmenkivi K, Myllarniemi M, Kinnula VL. 2008. Peroxiredoxin II expression and its association with oxidative stress and cell proliferation in human idiopathic pulmonary fibrosis. J. Histochem. Cytochem. 56:951–959. http://dx.doi.org/10.1369/jhc.2008.951806.

JOURNAL OF PROTEOMICS 111 (2014) 30–45

Available online at www.sciencedirect.com

ScienceDirect

www.elsevier.com/locate/jprot

Proteomic analysis of *Entamoeba histolytica* in vivo assembled pre-mRNA splicing complexes☆

Jesús Valdés[a,*], *Tomoyoshi Nozaki*[b], *Emi Sato*[b], *Yoko Chiba*[c], *Kumiko Nakada-Tsukui*[b], *Nicolás Villegas-Sepúlveda*[d], *Robert Winkler*[e], *Elisa Azuara-Liceaga*[f], *María Saraí Mendoza-Figueroa*[a], *Natsuki Watanabe*[c], *Herbert J. Santos*[b,c,g], *Yumiko Saito-Nakano*[b], *José Manuel Galindo-Rosales*[a]

[a]*Departament of Biochemistry, CINVESTAV, México D.F., Mexico*
[b]*Department of Parasitology, National Institute of Infectious Diseases, Tokyo, Japan*
[c]*University of Tsukuba, Graduate School of Life and Environmental Sciences, Tsukuba, Japan*
[d]*Department of Molecular Biomedicine, CINVESTAV, México D.F., Mexico*
[e]*Department of Biotechnology and Biochemistry, CINVESTAV Unidad Irapuato, Irapuato, Guanajuato, Mexico*
[f]*Posgrado en Ciencias Genómicas, UACM, México D.F., Mexico*
[g]*Institute of Biology, College of Science, University of the Philippines Diliman, Quezon City, Philippines*

ARTICLE INFO

Available online 8 August 2014

Keywords:
mRNP
Splicing
Splicing factors
Splice sites
DExH/A RNA helicases
Entamoeba histolytica

ABSTRACT

The genome of the human intestinal parasite *Entamoeba histolytica* contains nearly 3000 introns and bioinformatic predictions indicate that major and minor spliceosomes occur in *Entamoeba*. However, except for the U2-, U4-, U5- and U6 snRNAs, no other splicing factor has been cloned and characterized. Here, we HA-tagged cloned the snRNP component U1A and assessed its expression and nuclear localization. Because the snRNP-free U1A form interacts with polyadenylate-binding protein, HA-U1A immunoprecipitates could identify early and late splicing complexes. Avoiding *Entamoeba*'s endonucleases and ensuring the precipitation of RNA-binding proteins, parasite cultures were UV cross-linked prior to nuclear fraction immunoprecipitations with HA antibodies, and precipitates were subjected to tandem mass spectrometry (MS/MS) analyses. To discriminate their nuclear roles (chromatin-, co-transcriptional-, splicing-related), MS/MS analyses were carried out with proteins eluted with MS2–GST–sepharose from nuclear extracts of an MS2 aptamer-tagged Rabx13 intron amoeba transformant. Thus, we probed thirty-six *Entamoeba* proteins corresponding to 32 cognate splicing-specific factors, including 13 DExH/D helicases required for all stages of splicing, and 12 different splicing-related helicases were identified also. Furthermore 50 additional proteins, possibly involved in co-transcriptional processes were identified, revealing the complexity of co-transcriptional splicing in *Entamoeba*. Some of these later factors were not previously found in splicing complex analyses.

Biological significance
Numerous facts about the splicing of the nearly 3000 introns of the *Entamoeba* genome have not been unraveled, particularly the splicing factors and their activities.

☆ This article is part of a Special Issue entitled: Proteomics, mass spectrometry and peptidomics, Cancun 2013. Guest Editors: César López-Camarillo, Victoria Pando-Robles and Bronwyn Jane Barkla.

* *Corresponding author.*
E-mail address: jvaldes@cinvestav.mx (J. Valdés).

http://dx.doi.org/10.1016/j.jprot.2014.07.027

Considering that many of such introns are located in metabolic genes, the knowledge of the splicing cues has the potential to be used to attack or control the parasite.
We have found numerous new splicing-related factors which could have therapeutic benefit. We also detected all the DExH/A RNA helicases involved in splicing and splicing proofreading control. Still, *Entamoeba* is very inefficient in splicing fidelity, thus we may have found a possible model system to study these processes.
This article is part of a Special Issue entitled: Proteomics, mass spectrometry and peptidomics, Cancun 2013. Guest Editors: César López-Camarillo, Victoria Pando-Robles and Bronwyn Jane Barkla.

1. Introduction

The vast majority of early branching eukaryotes have few or no introns at all. However, around 3 thousand introns have been identified within the 9938 reported genes of the protozoa *Entamoeba histolytica* [1], and only a few of them have been validated [2–9].

The introns of *Entamoeba* possess conserved 5′ (GUUUGU) and 3′ (UAG) splice sites (ss), respectively, but the branch point sequences (BS) lack such degree of conservation [8]. These sites are recognized in a stepwise orderly fashion to assemble the spliceosome and conform the catalytic site(s) responsible for the excision of an intron of a pre-mRNA and ligation of its flanking exons (reviewed in Ref. [10]). First, the U1 small nuclear ribonucleic particle (snRNP) interacts with the conserved 5′ss of the pre-mRNA whereas both small and large subunits of the U2 auxiliary factor, U2AF, interact with the 3′ss forming the spliceosomal E complex. In the next step the U2 snRNP stably interacts with the pre-mRNA's branch site, leading to the A complex (i.e., prespliceosome). The A complex then interacts with the preformed *U4/U6 · U5 tri*-snRNP particle giving place to the precatalytic B complex, which will undergo RNP rearrangements, including loss of U1 and U4 snRNPs, thus converted in an activated B* complex which will carry out the first step of splicing (i.e. a nucleophilic attack of the BS adenosine at the 5′ss) generating a 3′ exon–lariat intron intermediary and a cleaved 5′ exon. Finally, the C complex that catalyzes the second step of splicing, excising the intron and ligating the 5′ and 3′ exons is formed, thus producing a mature mRNA in form of a RNP suitable for translation. RNA–RNA interactions are mainly responsible in spliceosome remodeling and catalytic core conformation [11–13] and numerous proteins are also required for assembly and splicing catalysis and splicing fidelity as well [14–16]. Participating factors of mainly human and yeast have been determined by mass spectrometry (MS) of in vitro assembled and affinity-purified spliceosomal complexes of model pre-mRNAs [17–29]. Over 150 proteins have been recruited in such complexes and this repertoire has been extended when the analysis was carried out from yeast, human and chicken cellular spliceosomes [30].

Most *Entamoeba* pre-mRNAs are mono-intronic although bioinformatic analyses predict that intron retention might be the main route for alternative splicing events [2,31] in agreement with the RT-PCR analyses of validated introns (see above), suggesting that rather than proteome expansion, splicing might constitute another layer of gene expression regulation. In spite of this, little is known of the *E. histolytica* spliceosomal components, and much less about their functions. Recently, the amoebic U2, U4, U5 and U6 snRNAs have been identified [2,32]. Furthermore, the *Entamoeba* major and minor spliceosomal components [33], as well as DExH/D-box helicases, some of which are known to be involved in pre-mRNA splicing, and processing [4], have been bioinformatically deduced. The lack of functional information restricts comparative studies of *Entamoeba* spliceosome components as much as our understanding of the lesser conservation of spliceosome proteins between *E. histolytica* and humans than between *Entamoeba dispar* and humans. Therefore, direct biochemical approaches are required to characterize the *E. histolytica* spliceosomal orthologs that will provide insights into the pre-mRNA splicing control, and will help to understand additional gene expression regulation events of *E. histolytica* biology.

To search for the *E. histolytica* RNA-binding early complex splicing factors in a supra/polyspliceosomal context [34], a main component of the U1 snRNA, protein U1A was HA tag-cloned and used in UV cross-linking immunoprecipitation (CLIP) assays with anti-HA antibodies from nuclear fractions of HA-U1A and mock amoeba transfectants. The resulting immunoprecipitates were subjected to MS/MS analysis. This protein dataset was confirmed and complemented with the one obtained from immunoprecipitates of amoeba transformed with an aptamer-tagged test intron. Although our experimental design does not provide stoichiometric data and may not be sensitive enough to identify low abundance pre-mRNA-specific factors, it allowed us to probe 36 *Entamoeba* splicing components (corresponding to 32 cognate splicing proteins), 12 splicing-related helicases, and 50 nuclear pre-mRNA-complex components.

2. Materials and methods

2.1. *Entamoeba* cultures

Trophozoites of *E. histolytica* strain HM-1:IMSS Cl-6 were cultured axenically at 35 °C in 13 × 100 mm screw-capped Pyrex glass tubes or plastic culture flasks in BI-S-33 medium as previously described [35,36].

2.2. Constructs and amoeba transfectants

The protein coding regions of U1A, RabX13, and RabC1, and the N-terminus of the human influenza virus NS1 (nNS1) genes were amplified by PCR from cDNA or genomic DNA (RabX13 clones) using their respective oligonucleotide pairs (5′ → 3′): U1AF (CACACCCGGGATGGAACAAGAAGAAGATAAAAAAAA) and U1AR (GTAAC TCGAGTCAATTAGCAAACTGGAGTATTA